JGR Oceans

RESEARCH ARTICLE
10.1029/2021JC017292

Key Points:

- 70%–80% of the dissolved organic carbon (DOC) exported from the tropical peatlands is remineralized in the Sunda Shelf Sea
- This drives a seasonal decline in pH by 0.1 and a net CO_2 efflux of 2.4–4.9 mol m^{-2} yr^{-1} in the central Sunda Shelf
- 20%–30% of the peatland-derived DOC might be relatively refractory and exported to the open Indian Ocean

Supporting Information:

Supporting Information may be found in the online version of this article.

Correspondence to:

Y. Zhou and P. Martin,
zhou0303@e.ntu.edu.sg;
pmartin@ntu.edu.sg

Citation:

Zhou, Y., Evans, C. D., Chen, Y., Chang, K. Y. W., & Martin, P. (2021). Extensive remineralization of peatland-derived dissolved organic carbon and ocean acidification in the Sunda Shelf Sea, Southeast Asia. *Journal of Geophysical Research: Oceans*, *126*, e2021JC017292. https://doi.org/10.1029/2021JC017292

Received 18 FEB 2021
Accepted 28 MAY 2021

Author Contributions:

Conceptualization: Patrick Martin
Data curation: Yongli Zhou, Yuan Chen, Kristy Y. W. Chang, Patrick Martin
Formal analysis: Yongli Zhou
Funding acquisition: Patrick Martin
Investigation: Yongli Zhou, Yuan Chen, Kristy Y. W. Chang
Methodology: Yongli Zhou, Yuan Chen
Project Administration: Yongli Zhou, Patrick Martin
Software: Yongli Zhou

Extensive Remineralization of Peatland-Derived Dissolved Organic Carbon and Ocean Acidification in the Sunda Shelf Sea, Southeast Asia

Yongli Zhou[1], Christopher D. Evans[2], Yuan Chen[1], Kristy Y. W. Chang[1,3], and Patrick Martin[1]

[1]Asian School of the Environment, Nanyang Technological University, Singapore, Singapore, [2]UK Centre for Ecology and Hydrology, Bangor, UK, [3]Now at Singapore Centre for Environmental Life Sciences Engineering, Nanyang Technological University, Singapore, Singapore

Abstract Southeast Asia is a hotspot of riverine export of terrigenous organic carbon to the ocean, accounting for ~10% of the global land-to-ocean riverine flux of terrigenous dissolved organic carbon (tDOC). While anthropogenic disturbance is thought to have increased the tDOC loss from peatlands in Southeast Asia, the fate of this tDOC in the marine environment and the potential impacts of its remineralization on coastal ecosystems remain poorly understood. We collected a multi-year biogeochemical time series in the central Sunda Shelf (Singapore Strait), where the seasonal reversal of ocean currents delivers water masses from the South China Sea first before (during Northeast Monsoon) and then after (during Southwest Monsoon) they have mixed with run-off from peatlands on Sumatra. The concentration and stable isotope composition of DOC, and colored dissolved organic matter spectra, reveal a large input of tDOC to our site during Southwest Monsoon. Using isotope mass balance calculations, we show that 60%–70% of the original tDOC input is remineralized in the coastal waters of the Sunda Shelf, causing seasonal acidification. The persistent CO_2 oversaturation drives a CO_2 efflux of 2.4–4.9 mol m^{-2} yr^{-1} from the Singapore Strait, suggesting that a large proportion of the remineralized peatland tDOC is ultimately emitted to the atmosphere. However, incubation experiments show that the remaining 30%–40% tDOC exhibits surprisingly low lability to microbial and photochemical degradation, suggesting that up to 20%–30% of peatland tDOC might be relatively refractory and exported to the open ocean.

Plain Language Summary Peatlands are large stores of organic carbon and are extensively distributed across coastal Sumatra and Borneo in Southeast Asia. These peatlands give rise to a large flux of dissolved organic carbon (DOC) via rivers to the Sunda Shelf Sea, the marginal sea in Southeast Asia, and land conversion of peatlands has likely increased this flux. In the marine environment, organic carbon can be remineralized to CO_2 by sunlight and by microbial respiration, but the fate of peatland tDOC in coastal waters of Southeast Asia remains unclear. In this study, we analyzed water samples collected from the Sunda Shelf and found that 60%–70% of the DOC from peatlands is decomposed to CO_2 in the coastal waters of the shelf sea. We further found that this resulted in a decrease in seawater pH by 0.10, and that a large proportion of the CO_2 is probably emitted to the atmosphere. This implies that the reported increase in tDOC export due to peatland disturbance may have had a significant effect on coastal biogeochemistry and downstream greenhouse gas emissions.

1. Introduction

Southeast Asia harbors the largest area of the world's tropical peatlands, which are widely distributed in coastal areas of Sumatra and Borneo and store around 69 Pg C of terrestrial organic carbon (Dommain et al., 2014; Page et al., 2011). Consequently, Southeast Asia is also a hotspot of terrestrial organic carbon export to the ocean: the fluvial flux of terrigenous dissolved organic carbon (tDOC) to the Sunda Shelf Sea is ~21 Tg C yr^{-1}, which accounts for ~10% of the annual global land-to-ocean tDOC flux by the world's rivers (Baum et al., 2007; Moore et al., 2011). In addition, most of this peatland area has been anthropogenically disturbed by deforestation and land conversion (Miettinen et al., 2016), which is thought to have increased the peatland tDOC export to the ocean by 32% over the past three decades (Moore et al., 2013; Yupi

Supervision: Christopher D. Evans, Patrick Martin
Visualization: Yongli Zhou, Yuan Chen
Writing – original draft: Yongli Zhou, Christopher D. Evans, Yuan Chen, Kristy Y. W. Chang, Patrick Martin
Writing – review & editing: Yongli Zhou, Christopher D. Evans, Patrick Martin

et al., 2016). This ongoing anthropogenic pressure on peatlands could therefore have impacts extending into the marine environment of Southeast Asia, especially on sensitive ecosystems such as coral reefs.

Our understanding of the biogeochemical fate of tDOC in the global oceans is still limited, and in particular, the degree to which ocean margins are efficient filters or conduits of tDOC between land and ocean remains debated. On the one hand, numerous studies have indicated that tDOC can be extensively and rapidly remineralized within ocean margins, as reported for the North Sea (Kitidis et al., 2019; Painter et al., 2018), the Louisiana Shelf (Fichot & Benner, 2014), and the Arctic Shelf (Alling et al., 2008; Humborg et al., 2017; Kaiser et al., 2017; Letscher et al., 2011; Semiletov et al., 2016). Remineralization of tDOC fuels strong CO_2 emissions from coastal waters (Cai, 2011; Chen & Borges, 2009; Roobaert et al., 2019) and causes acidification in shelf seas (Capelle et al., 2020; Semiletov et al., 2016). This is consistent with the canonical view that the DOC pool in the deep oceans only contains trace amounts of terrigenous DOC, as indicated by the low lignin concentrations (Meyers-Schulte & Hedges, 1986; Opsahl & Benner, 1997). On the other hand, some studies suggest that tDOC sometimes undergoes more limited remineralization within the ocean margins, and that a correspondingly larger proportion is delivered to the open oceans. For example, Medeiros et al. (2015) found that 50%–76% of the tDOC exported by the Amazon River reaches the open Atlantic Ocean, likely due to the rapid transport of tDOC across the shelf. This might also be linked to the prior degradation history of tDOC before reaching the sea, as removal of the most labile fractions may result in the remaining tDOC having only limited degradability in some river systems (Chupakova et al., 2018; Shirokova et al., 2019; Stubbins et al., 2017; N. D. Ward et al., 2013). Recent molecular evidence shows that some fractions of tDOC are refractory and are exported to the open ocean (Cao et al., 2018; Medeiros et al., 2016), and carbon isotope data suggest that the terrestrial contribution to the oceanic DOC pool might be up to 30%, which is higher than previously believed (Follett et al., 2014; Zigah et al., 2017). It therefore remains unclear exactly how much tDOC is remineralized within ocean margins globally, with the extent of tDOC remineralization likely depending on factors such as the composition of the tDOC and the water circulation across the shelf, and varying substantially between different regions. However, most research has hitherto focused on mid- to high-latitude regions, and more research is therefore needed in tropical shelf seas that are the recipients of some of the highest rates of tDOC input globally.

The peatland-draining rivers in Southeast Asia are characterized by very high DOC concentrations (1,000–5,000 μmol L^{-1}) and high colored dissolved organic matter (CDOM a_{350}, 50–200 m^{-1}) (Alkhatib et al., 2007; Martin et al., 2018; Moore et al., 2011; Rixen et al., 2008; Wit et al., 2015, 2018), which are among the highest values found in rivers globally (Meybeck, 1982). However, these peat-draining rivers only show moderate-to-low CO_2 efflux relative to their high DOC concentrations (Müller et al., 2015; Müller-Dum et al., 2019; Wit et al., 2015), and recent experimental data suggest that Southeast Asian peatland DOC is relatively refractory to microbial decomposition (Nichols & Martin, 2021). In addition, field surveys have typically revealed conservative mixing of DOC across peatland-draining river estuaries (Alkhatib et al., 2007; Martin et al., 2018; Rixen et al., 2008; Wit et al., 2015; Zhou et al., 2019). This suggests that remineralization of tDOC within the rivers is limited, possibly due to lack of oxygen, low pH, and short water residence times (Wit et al., 2015), which means that a large proportion of the peatland-derived tDOC is presumably exported to the coastal sea. Consistent with this prediction, Zhou et al. (2019) estimated from fluorescent dissolved organic matter data that 20%–40% of the bulk DOC pool in coastal waters of northwestern Borneo (with salinity >30) is of terrestrial origin, due to the large input of peatland tDOC. It is possible that a large proportion of this tDOC is remineralized after it is exported to the coastal waters, as suggested by the high photo-lability of Southeast Asian peatland tDOC (Martin et al., 2018; Rixen et al., 2008) and the large CO_2 emissions reported for the coastal waters of eastern Sumatra (Wit et al., 2018). Given the large scale of the potential anthropogenic perturbation to the peatland tDOC flux, it is particularly important to better constrain the biogeochemical fate of this tDOC and the associated impacts on both the shelf sea environment and the atmospheric greenhouse gas budget through the air-sea CO_2 exchange.

Here, we analyzed a multi-year time series of DOC, carbonate system parameters, and carbon stable isotope composition using a mass balance approach to quantify the remineralization of peatland-derived tDOC in the Sunda Shelf. The seasonal acidification in the shelf sea and CO_2 emissions driven by the tDOC remineralization were further quantified. Laboratory decomposition experiments were performed to investigate the degradability of peatland-derived tDOC and estimate tDOC export to the open ocean.

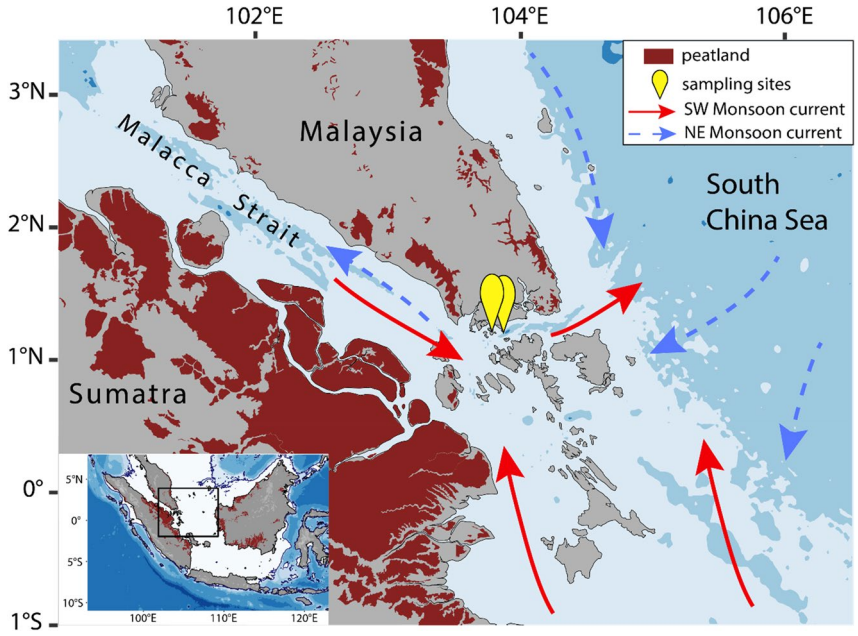

Figure 1. Map of the study region showing the location of tropical peatlands, the time series sampling site in the Singapore Strait and the directions of the prevailing ocean currents across the Sunda Shelf Sea. During the Northeast (NE) Monsoon season, the currents transport water from the open South China Sea to our study site; during the Southwest (SW) Monsoon season, the currents reverse and deliver water with inputs from the tropical peatlands along the east coast of Sumatra to our site, resulting in the seasonal variations in biogeochemistry.

2. Materials and Methods

2.1. Study Area

We collected biogeochemical timeseries data at two sites in the Singapore Strait, Kusu Island (1.226°N, 103.860°E) and Hantu Island (1.227°N, 103.747°E). Both sites have coral reefs with >70 species of hard coral and coral cover of around 40%–50% (Bauman et al., 2017; Huang et al., 2009; Januchowski-Hartley et al., 2020). The Singapore Strait is located in the center of the Sunda Shelf Sea, and is close to the coastal peatlands on Sumatra (Figure 1), with water depth mostly less than 40 m. The annual average circulation runs from the South China Sea into the Indian Ocean through the Java Sea and the Malacca Strait (Gordon et al., 2012). However, the monsoon system causes the main ocean currents to reverse direction seasonally (Figure 1) (Mayer & Pohlmann, 2014; Mayer et al., 2018). During the Northeast Monsoon (November to February), water flows from the South China Sea westwards through the Singapore Strait and along the coast of Sumatra. During the Southwest Monsoon (May to September), the currents reverse and flow back eastwards through the Singapore Strait, carrying river discharge from the Sumatran peatlands (Mayer & Pohlmann, 2014; Siegel et al., 2019). Water in the Malacca and Singapore Straits is well mixed due to strong tidal currents (Mayer & Pohlmann, 2014). Because spatial variability between our two sampling sites was much smaller than the seasonal variability, we do not distinguish the data by site in this analysis.

2.2. Collection of Water Samples

Water samples were collected from both stations 1–2 times per month using a 1.5 L Niskin bottle at 5 m depth from October 2017 until August 2020. The water was immediately filtered on the boat through a pre-rinsed 47 mm diameter, 0.22 μm pore-size polyethersulfone membrane filter (Supor, Merck Millipore) in an in-line filter housing connected to a peristaltic pump and preserved for analyses of DOC, CDOM spectra, dissolved inorganic carbon (DIC), total alkalinity (TA), stable isotope composition of DOC ($\delta^{13}C_{DOC}$) and of DIC ($\delta^{13}C_{DIC}$), and dissolved inorganic nutrients (methods of collection are summarized in Table 1). Samples were all stored dark before analysis. The filter housing was bled of any air bubbles before collecting samples. Samples for chlorophyll-*a* were filtered onto 25 mm diameter Whatman GF/F filters instead, kept

Table 1
Collection and Preservation of Each Biogeochemical Parameter After Filtration

Parameter	Collection method	Preservation temperature
$\delta^{13}C_{DIC}$	One milliliter of sample injected into a 12-ml Exetainer vial capped with butyl rubber septum containing 1 ml of ≥85% phosphoric acid and pre-flushed with helium.	20°C
DIC	A 12-ml Exetainer vial was filled to overflowing, left to overflow for 15 seconds, and capped immediately with a butyl rubber septum to prevent gas exchange.	4°C
TA	Collected into a 140-ml HDPE bottle.	4°C
$\delta^{13}C_{DOC}$	Filled 40 ml into a 50-ml polypropylene centrifuge tube and stored frozen. Samples were thawed and acidified with 37% hydrochloric acid immediately prior to being sent off for analysis.	−20°C
CDOM	Filled 30 ml into a 40-ml pre-combusted EPA borosilicate vial.	4°C
DOC	Filled 30 ml into a 40-ml pre-combusted EPA borosilicate vial, acidified with 100 μl of 50% sulfuric acid.	4°C
Dissolved inorganic nutrients	Filled 10 ml into a 15-ml polypropylene centrifuge tube and stored frozen.	−20°C

Abbreviations: CDOM, colored dissolved organic matter; DIC, dissolved inorganic carbon; DOC, dissolved organic carbon; TA, total alkalinity.

at −80°C and analyzed within 3 months of collection. At each station, a depth profile of salinity and temperature was measured by a fastCTD Profiler (Valeport Ltd).

2.3. Deployment of Autonomous Sensors

An SBE 19plus V2 SeaCAT CTD and a SeaFET pH sensor (both Sea-Bird Electronics, Inc.), equipped with copper biofouling guards, were deployed at Kusu Island in July 2015 to monitor seawater salinity, temperature, and pH every 10 minutes. A SAMI-CO_2 sensor (Sunburst Sensors), equipped with copper biofouling guards, was deployed at the same location from March 2018 until July 2019 to measure the partial pressure of CO_2 (pCO_2) every 2 hours. Sensors were attached horizontally to iron stakes hammered into the reef sediment at roughly 5 m depth along the reef slope and were retrieved every 1–3 months for data download and maintenance.

The sensor data were validated with the CTD profile measurements and our measurements of DIC and TA of water samples collected during each field cruise, using the MATLAB CO2SYS Package Version 2.0 (referred to as CO2SYS below) (Orr et al., 2018; van Heuven et al., 2011). The dissociation constants of Mehrbach et al. (1973) as refit by Dickson and Millero (1987) for carbonic acid and of Dickson (1990) for HSO_4^- and the total boron concentration of Uppström (1974) were used for CO2SYS. The sensor data are presented as daily mean values. Data gaps occurred whenever sensors were removed for maintenance or were sent for recalibration, or when biofouling or sensor drift caused deterioration in data quality (as determined by comparison to our CTD profile and laboratory measurements; these data were omitted). The data quality of the SAMI-CO_2 sensor was rapidly affected by biofouling and sediment accumulation despite testing different sample pump and copper fouling guard configurations, and we therefore stopped deploying it after July 2019. All seawater pH data are reported on the Total scale.

2.4. Sample Analysis

DIC was measured with an Apollo SciTech AS-C5 DIC analyzer at room temperature (22 ± 0.5°C) using an injection volume of 1 ml and a phosphoric acid solution of 3% v/v phosphoric acid with 7% w/v sodium chloride. The phosphoric acid was sparged with N_2 gas for 5 min prior to each analysis run. Each sample was measured 3–5 times to achieve a relative standard deviation of ≤0.1% for three replicate injections. Calibration was performed using the certified reference material (CRM) from Andrew Dickson's laboratory, Scripps Institution of Oceanography (Batch 172) or an in-house secondary standard made from Singapore Strait seawater that we calibrated against the CRM. The analytical precision for DIC was ±0.15% or lower based on replicate measurements of the CRM and the secondary standard.

TA was measured with an Apollo SciTech AS-ALK2 titrator, which automates the Gran titration (Gran, 1952), using a ROSS combination glass pH electrode (Orion 8302BNUMD). Samples and standards were warmed to room temperature (22 ± 0.5°C) and samples were measured 2–4 times in 25-ml aliquots using 0.1 M hydrochloric acid. The acid concentration was calibrated against the CRM or our in-house secondary standard. The analytical precision for TA was ±0.13% or lower based on replicate measurements of the CRM and the secondary standard.

Samples for DIC and TA were not poisoned with $HgCl_2$ but were all analyzed within 24 h after sampling, because two additional experiments we performed show that filtration with refrigeration is sufficient for preservation of samples from our sites for DIC and TA for 62 days (Text S1, Figure S3).

Absorption spectra of CDOM were measured from 230 to 900 nm against a reference of ultrapure deionized water (18.2 MΩ cm^{-1}, referred to as DI water below) using a Thermo Evolution 300 dual-beam spectrophotometer in a 10-cm quartz cuvette. The absorption coefficients, the spectral slope $S_{275–295}$ (Helms et al., 2008), and the specific UV absorbance at 254 nm, $SUVA_{254}$ (Weishaar et al., 2003), were calculated using the "hyperSpec" package in R (Beleites & Sergo, 2012). We express the CDOM concentration as the absorption coefficient at 350 nm, a_{350}.

DOC samples (30 ml) were acidified with 100 μl of 50% sulfuric acid and analyzed on a Shimadzu TOC-L system with a high-salt combustion kit, using an injection volume of 150 μl and a 5-min sparge time. Each sample was measured 5–7 times to achieve a coefficient of variation of ≤2%. Potassium hydrogen phthalate was used for calibration, and the analytical accuracy was monitored using certified deep-sea water reference material (42–45 μmol L^{-1} DOC) from the University of Miami, USA. Our analyses consistently yielded slightly higher values for the CRM, with a long-term mean and standard deviation of 48.0 ± 3.9 μmol L^{-1} DOC.

The $\delta^{13}C_{DOC}$ samples were thawed, acidified to pH of 2–3 with 37% w/v hydrochloric acid, and shipped to the Ján Veizer Stable Isotope Laboratory, University of Ottawa, Canada for analysis using an OI Analytical Aurora Model 1030W TOC Analyzer interfaced to a Finnigan Mat DeltaPlusXP isotope ratio mass spectrometer. The 2-sigma analytical precision is ±0.4‰ (https://isotope.uottawa.ca/en/services-waters).

$\delta^{13}C$ of DIC measurements were made using a Gas Bench connected to an isotope ratio mass spectrometer at the Stable Isotope Facility, University of California, Davis (UC Davis) and by ourselves at the Marine Geochemistry Laboratory, Nanyang Technological University, Singapore (NTU). At NTU, final $\delta^{13}C$ values were obtained after instrumental drift correction, blank correction for standards (Assayag et al., 2006; Humphreys et al., 2016), and calibration using NBS-18 ($\delta^{13}C = -5.01$‰) and Estremoz ($\delta^{13}C = 1.63$‰) calcium carbonate standards. All $\delta^{13}C$ values of the samples were further corrected by accounting for the difference between the international consensus value of $\delta^{13}C_{DIC}$ of the Dickson CRM (0.78‰) (Cheng et al., 2019) and our laboratory measurements of $\delta^{13}C_{DIC}$ of the Dickson CRM at NTU (the magnitude of this correction was mostly below 0.4‰). The standard deviation for $\delta^{13}C$ of DIC measurements over multiple years at UC Davis is reported as ±0.1‰ (https://stableisotopefacility.ucdavis.edu/) and at NTU was ±0.2‰ (Carrara marble, $n = 24$, 4 runs).

Chlorophyll-*a* was extracted in 90% acetone at 4°C in the dark for 24 h and measured on a HORIBA Floromax-4 fluorometer with excitation at 436 nm and emission at 680 nm, with bandpasses of 5 nm (Welschmeyer, 1994). Data were normalized to the reference signal and calibrated using a spinach chlorophyll-*a* standard (Sigma-Aldrich C5753).

Dissolved inorganic nutrients were analyzed on a SEAL AA3 segmented-flow analyzer using standard SEAL methods for seawater analysis, and the silicate and phosphate data were used for carbonate system calculation by CO2SYS (data not shown).

2.5. Analyses of the Time-Series Data

Due to the monsoonal current reversal, the Singapore Strait seasonally receives water directly from the South China Sea with little terrestrial influence. This water subsequently mixes with peat-draining river input off the coast of Sumatra, and then seasonally flows back into the Singapore Strait when the currents reverse direction (Figure 1). The seasonal variation in the Singapore Strait is therefore equivalent to the

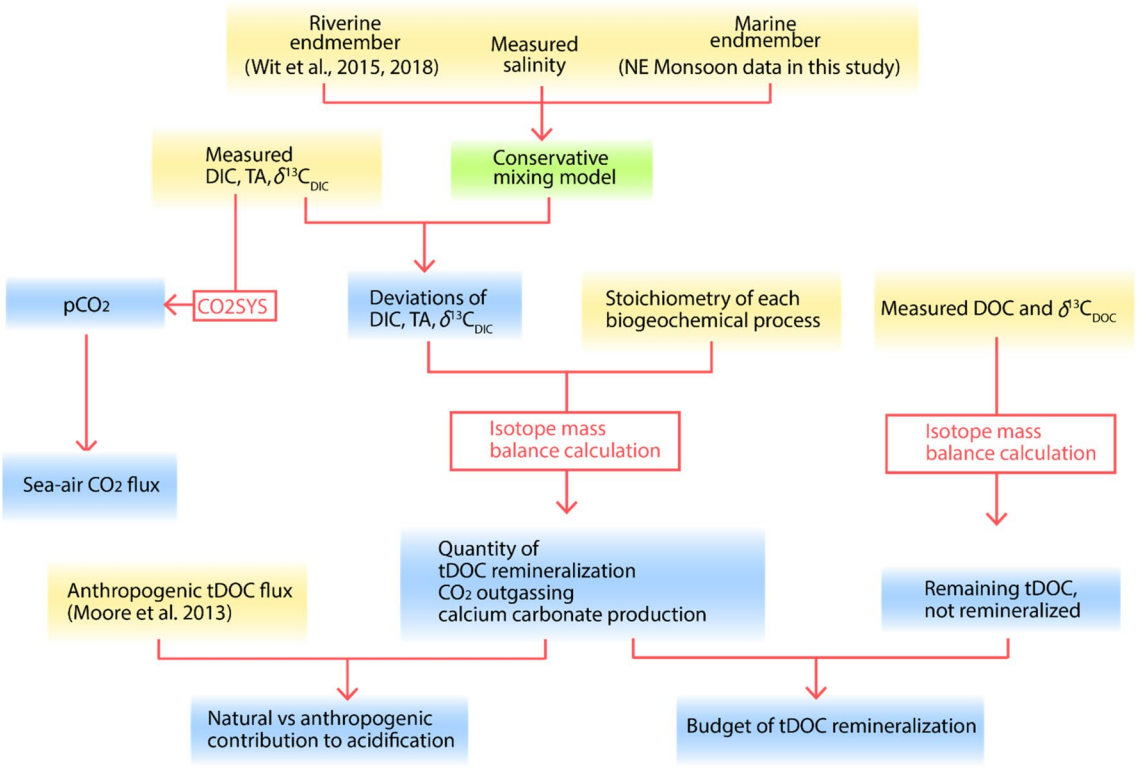

Figure 2. A flowchart summarizing the data analyses for this study. Yellow boxes indicate the inputs and blue boxes indicate outputs of calculations. We built a conservative mixing model to predict the biogeochemical parameters if there was only mixing between riverine water and marine water. Isotope mass balance calculations were performed with the deviations of the measured data from the mixing model to quantify tDOC remineralization and the potential anthropogenic contribution to the seasonal acidification. DIC, dissolved inorganic carbon; DOC, dissolved organic carbon; TA, total alkalinity; tDOC, terrigenous DOC.

spatial variability from the South China Sea into the coastal waters of Sumatra in the Malacca and Karimata Straits, and therefore reflects the mixing of water from the open sea with peatland-draining river input.

Our data analysis consists of two components: first, we built a conservative mixing model to predict the values of DIC, TA, pH, and $\delta^{13}C_{DIC}$ if this mixing was strictly conservative. We therefore interpret any deviations in our measurements relative to the predicted values as indicative of biogeochemical processing. Second, we performed isotope mass balance calculations for DOC and the carbonate system to estimate how much of the DOC pool was tDOC, how much of the excess DIC (relative to conservative mixing) was contributed from tDOC remineralization, and, when the measured deviations in $\delta^{13}C_{DIC}$ were greater than could be explained from the measured deviation in DIC concentration, how much additional tDOC must have been remineralized and already outgassed upstream of our site to explain the measured $\delta^{13}C_{DIC}$. These calculations are summarized in Figure 2 and below, and full details are provided in Text S2.

2.5.1. Conservative Mixing Model

We built a two-endmember mixing model to calculate the DIC, TA, pH, and $\delta^{13}C_{DIC}$ expected from conservative mixing between the riverine endmember and the marine endmember. This allowed us to calculate the deviations of the measured data from the values expected from conservative mixing. The relative contribution of riverine input and marine input was calculated from the measured salinity. Seawater pH expected from conservative mixing was calculated from the DIC and TA of conservative mixing by CO2SYS.

We calculated the discharge-weighted average of the published data of DIC, TA (calculated from pH and pCO_2), and $\delta^{13}C_{DIC}$ from the main peat-draining rivers on Sumatra (the Batanghari, Indragiri, Kampar, and Siak Rivers) (Figure S1) (Wit et al., 2015, 2018), which we adopted as the riverine endmember values. The marine endmember values were estimated from our measurements in the Singapore Strait from the end of the NE Monsoon and the subsequent inter-monsoon season (late February–March), when the water in the

Table 2
Endmember Values (±1SD) and the Uncertainties (Shown as ±1SD) of the Parameters Measured at Our Site as Input to the Conservative Mixing Model and Monte Carlo Uncertainty Calculation

Parameter	Riverine endmember	Marine endmember	Uncertainty of measured data
Salinity	0	32.69 ± 0.23	±0.01
DIC (μmol kg^{-1})	453 ± 34	1,903 ± 13	±0.15%
TA (μmol kg^{-1})	310 ± 34	2,164 ± 15	±0.13%
$\delta^{13}C_{DIC}$ (‰)	−15.32 ± 1	−0.25 ± 0.09	±0.2
$\delta^{13}C_{DOC}$ (‰)	−29 ± 1	−21.88 ± 0.79	±0.2
$\delta^{13}C_{tDIC}$ (‰)[a]	−32 ± 1	-	-
DOC (μmol L^{-1})[b]	-	-	±3.9

Abbreviations: DIC, dissolved inorganic carbon; DOC, dissolved organic carbon; TA, total alkalinity; tDOC, terrigenous DOC.
[a]The $\delta^{13}C$ of DIC produced from remineralization of peatland-derived tDOC. [b]DOC endmember values were not used in the calculations.

Singapore Strait consists predominantly of marine water from the open South China Sea and our data indicated minimal presence of tDOC and freshwater input (Section 3.1). All the endmember values and the uncertainties are provided in Table 2.

2.5.2. Isotope Mass Balance Calculations

Based on the known changes in DIC, TA, and $\delta^{13}C_{DIC}$ relative to the values expected from conservative mixing caused by primary production, remineralization, calcium carbonate production and dissolution and air-sea CO_2 exchange (Zeebe & Wolf-Gladrow, 2001) (Table S1), we back-calculated the amount of carbon that had been processed by these biogeochemical processes from the measured deviations in DIC, TA, and $\delta^{13}C_{DIC}$ using an isotope mass balance approach following Samanta et al. (2015). The proportion of the bulk DOC pool that was tDOC was calculated from the measured $\delta^{13}C_{DOC}$ and DOC concentration.

The $\delta^{13}C_{DOC}$ data were not available for rivers on Sumatra, but the $\delta^{13}C_{DOC}$ values of the peatland-derived tDOC across peatlands on Sumatra and rivers on Borneo and Peninsular Malaysia mostly range between −30 and −28‰ (Baum, 2008; Evans et al., 2014; Gandois et al., 2014; Zhu et al., 2020). We therefore adopted −29‰ as the riverine endmember value of $\delta^{13}C_{DOC}$ for the peatland-derived tDOC. For the $\delta^{13}C$ of the DIC produced from remineralization, microbial respiration causes little carbon isotopic fractionation, while results from our experiments (Section 3.6) and previous studies (Opsahl & Zepp, 2001; Osburn et al., 2001; Spencer et al., 2009) indicated that photodegradation (and combined photo-bio-degradation) of tDOC can cause fractionation in $\delta^{13}C$ of −1.4 to −5.8‰ between the produced DIC and the initial DOC (Table S2). Because of the low bio-degradability (Nichols & Martin, 2021) but high photo-degradability of Southeast Asian peatland tDOC (Section 3.6), we infer that a major part of the remineralization of tDOC in this region might be via photodegradation, and therefore entails a carbon isotopic fractionation. We adopted a fractionation of −3‰, and thus used −32‰ as the $\delta^{13}C$ of the DIC produced from tDOC remineralization. Note that by assuming this additional fractionation, our calculated amount of remineralized tDOC is smaller, since a smaller amount of carbon is needed to yield the observed $\delta^{13}C_{DIC}$ values.

These mass balance calculations provide the quantity of (a) the amount of tDOC at our site, representing the remaining fraction of the tDOC input from peatlands that has not been remineralized, (b) the remineralized tDOC as DIC, (c) the remineralized tDOC that had been removed by outgassing from the DIC pool upstream of our sampling site, and (d) the amount of calcium carbonate production and dissolution. The sum of the fractions (a–d) represents the initial concentration of tDOC for a given salinity after estuarine mixing and before biogeochemical processing has occurred.

The uncertainty of the mass balance calculations was estimated by a Monte Carlo algorithm, in which we perturbed each input parameter with a 1σ normally distributed error (Table 2) by random sampling, repeated the calculations 10,000 times, and then calculated the resulting standard deviation of each output parameter. For the riverine endmember values as input parameters, the 1σ error of the DIC and TA were adopted from Wit et al. (2018); the 1σ error of the $\delta^{13}C_{DIC}$ and $\delta^{13}C_{DOC}$ were both assumed to be ±1‰, because the uncertainties are not available and the reported $\delta^{13}C_{DOC}$ values of the peatland-derived tDOC in Southeast Asia mostly range between −30 and −28‰. The 1σ error of the marine endmember variables are the standard deviations of the measurements from late February to March. The 1σ error of the measured DOC, DIC, TA, $\delta^{13}C_{DIC}$, and $\delta^{13}C_{DOC}$ are the long-term 1σ precision of measurements of the standard materials. The 1σ error of the measured salinity (±0.01) was estimated based on the accuracy of the conductivity measurement of the Valeport fastCTD (±0.01 mS cm^{-1}).

2.5.3. Acidification and Putative Anthropogenic Contribution

Seasonal acidification was indicated by the time series measurements of DIC and TA and the SeaFET pH sensor data (Section 3.5). Saturation states of calcite and aragonite were calculated from the DIC and TA

data using CO2SYS. The uncertainties were estimated from the uncertainties of DIC, TA, and equilibrium constants using CO2SYS.

From the results of the mass balance calculations, we further reconstructed the individual contribution to the deviations of DIC and TA from (a) calcium carbonate dissolution, (b) remineralization of natural tDOC, and (c) remineralization of anthropogenic tDOC. The reconstructed DIC and TA deviations were translated to the pH deviations relative to conservative mixing by CO2SYS for assessment of the putative anthropogenic contribution to the observed acidification. We distinguished the natural tDOC remineralization from the anthropogenic component based on the report that 35% of the tDOC flux is caused by peatland perturbations (Moore et al., 2013). This estimate is based on a limited and small-scale comparison of disturbed and intact peatland catchments but agrees with the independent data-based modeling estimate by Rixen et al. (2016) that peatland DOC fluxes to the ocean have increased from 62.5 to 96 g m^{-2} yr^{-1}. Numerous subsequent studies have therefore applied this estimate that 35% of present-day peatland DOC flux is anthropogenic (Evans et al., 2016; Wilson et al., 2016; Wit et al., 2018).

2.5.4. Sea-Air CO_2 Flux

We calculated the annual areal sea-air CO_2 flux following Lønborg et al. (2019) using the seawater pCO_2 calculated from the measured DIC and TA (the in situ sensor record was too limited to be used) and the atmospheric pCO_2 measured at Bukit Kotobatang, Indonesia in 2019 (403.39–409.57 μatm, we used the annual average 406.60 μatm for calculation) (Dlugokencky et al., 2021). We obtained average wind speeds for the area of 0.5°N–1.5°N and 102.5°E–105.5°E from the CYGNSS Level 2 Science Data Record Version 2.1 (CYGNSS, 2017). The gas transfer velocity was calculated following Wanninkhof (2014). The CO_2 solubility was calculated following Weiss (1974) using the measured water temperature. The uncertainty of the CO_2 flux was estimated by a Monte Carlo algorithm, based on the uncertainty of the salinity, DIC, and TA measurements (Table 2) and the reported uncertainty of the gas transfer velocity (i.e., ±20%) (Wanninkhof, 2014).

2.6. Degradation Experiments

Incubation experiments were performed to determine the degradability of tDOC by photo-chemical remineralization and by microbial remineralization. For photo-chemical remineralization, we additionally measured the carbon isotopic fractionation.

For photodegradation experiments, surface water samples (<1 m depth) were collected from the Maludam River in Malaysia (1.636°N 111.049°E), which drains a large area of intact peatland on northwestern Borneo, in December 2018 and June 2019, and from Kusu Island in the Singapore Strait in January 2020 (NE Monsoon) and July 2020 (SW Monsoon). Samples were filtered through pre-rinsed Whatman Polycap filters or 0.22 μm pore-size polyethersulfone membrane filters on the day of collection, stored at 4°C and re-filtered prior to the experiments.

For the filtered water collected from the Maludam River in December 2018 and from the Singapore Strait, we filled 30 ml aliquots into replicate cylindrical quartz cells (50 mm pathlength, 50 mm diameter, with Teflon screw caps) and irradiated the samples in an Atlas Suntest CPS + solar simulator fitted with a xenon lamp and daylight optical filter. The temperature control was set to 40°C (the lowest possible setting), and light output between 300–400 nm was set to 40 W m^{-2}. The quartz cells were opened and ventilated regularly to avoid depletion of oxygen and then recapped. A dark control was prepared by filling 200 ml filtered water into a 250 ml Duran glass bottle, which was wrapped in aluminum foil and placed in the solar simulator. One or two replicate quartz cells were removed at regular time-points to measure DOC and CDOM (using 2-mm, 1-cm, or 10-cm pathlength quartz cuvettes) with parallel measurements of the dark control.

To measure carbon isotopic fractionation associated with photodegradation, the filtered water collected from the Maludam River in June 2019 was filled into replicate 150-ml quartz bottles with ground stoppers, leaving 30 ml headspace, and placed in an unshaded outdoor location at Nanyang Technological University, Singapore. Weather conditions during the experiment were partly sunny on most days, sometimes with heavy rain showers lasting up to a few hours. The ambient temperature varied between 26°C and 32°C within a diurnal cycle. The quartz bottles were opened and ventilated once a week to avoid oxygen depletion and then recapped. A dark control was prepared as above, and placed in the same location. One replicate

bottle was removed to measure DOC, CDOM (using 2-mm or 1-cm pathlength quartz cuvettes) and $\delta^{13}C_{DOC}$ on Days 0, 60, and 98, with parallel measurements of the dark control.

For the biodegradation experiment, 10 L of surface water (<1 m depth) was collected from Kusu Island in the Singapore Strait in July 2020 (SW Monsoon), part of which was kept unfiltered as an inoculum while the rest was filtered through 0.22 μm pore-size polyethersulfone membrane filters 1 day after collection. Three treatments were created: filtered water only (as sterile control), filtered water + inoculum (v/v = 5%), and filtered water + inoculum + labile DOC (leucine and glucose, each contributed approximately 10 μmol L^{-1} carbon, to test for a possible priming effect). For each treatment, replicate 150 ml aliquots of the appropriate water sample were filled into 250-mL Duran glass bottles, capped with airtight Teflon screw caps, and kept in the dark in a shaded outdoor location at Nanyang Technological University, Singapore. The ambient temperature varied between 26°C and 32°C within a diurnal cycle. Bottles were gently swirled every other day. For each treatment, three replicate samples were removed and filtered through 0.22 μm pore-size polyethersulfone membrane filters for DOC and CDOM measurements on Days 0, 3, 7, 14, 27, 48, and 109. Bottles were cleaned with 10% hydrochloric acid and DI water and combusted at 450°C for 4 h before use.

3. Results

3.1. Monsoon-Driven Seasonal Variation of tDOC Input to the Singapore Strait

During the SW Monsoon, the currents transport water from the east coast of Sumatra and the Malacca Strait to our sampling site in the Singapore Strait. These waters receive large riverine inputs from the extensive peatlands on Sumatra, and correspondingly we observed a decrease in salinity from ~33 to ≤30 during this period (Figure 3a, Figure S2a). The DOC concentration increased to 75–100 μmol L^{-1} (Figure 3c). The CDOM absorption (a_{350}) increased to 0.5–2 m^{-1} (Figure 3d). In addition, the SW Monsoon exhibited the lowest spectral slope of CDOM ($S_{275-295}$) (0.016–0.020 nm^{-1}), the highest $SUVA_{254}$ (2–3 L mg^{-1} m^{-1}), and the lightest $\delta^{13}C_{DOC}$ (−25.5 to −24‰) of the year, all of which indicate a large input of tDOC (Figures 3e–3g). The mass balance calculations showed that 20%–50% of the DOC pool in the Singapore Strait was terrigenous during this period (Figure 3h).

During the early NE Monsoon (December–January), when the water flows from the South China Sea, we also observed a brief decrease in salinity by ~2 units. Because this is the time of year with the greatest precipitation in Singapore and southern Malaysia, some freshwater input from run-off would be expected at this time. However, the DOC and CDOM concentrations, the $SUVA_{254}$, the $S_{275-295}$, and the $\delta^{13}C_{DOC}$ only showed small changes relative to the inter-monsoon periods (Figures 3c–3g), which suggest that the tDOC input was limited. During the late NE Monsoon and the following inter-monsoon season (late February–March; the season with lowest local precipitation), continuous water flow from the open South China Sea results in the highest salinity of the year (~32–33), low DOC concentration (~65 μmol L^{-1}), low a_{350} (<0.25 m^{-1}), high $S_{275-295}$ (>0.026 nm^{-1}), and more enriched values of $\delta^{13}C_{DOC}$ (−23 to −21‰) (Figures 3c–3g). We therefore took the averages of our data during this period as the marine endmember values for the conservative mixing model (Table 2).

The seawater temperature showed only a small seasonal variation, mostly between 28°C and 31°C (Figure 3b). The chlorophyll-*a* concentration mostly ranged between 0.5 and 2 μg L^{-1} and showed no clear seasonal variation (Data Set S1).

3.2. Seasonal Variation of DIC, TA, and $\delta^{13}C_{DIC}$ Driven by tDOC Remineralization

During the SW Monsoon, the DIC was mostly 15–40 μmol kg^{-1} higher than the values expected from the conservative mixing model, while the TA typically showed a depletion of 10–40 μmol kg^{-1} relative to conservative mixing (Figures 4a and 4b). By comparing the measured deviations with the known changes caused by different biogeochemical processes, we found that the variation in DIC and TA during the SW Monsoon was chiefly the result of remineralization and calcium carbonate production (Figure 4c). Because the Singapore Strait was always oversaturated with respect to pCO_2 (Section 3.4), net CO_2 outgassing, instead of CO_2 invasion, is expected throughout the year. Because CO_2 outgassing and calcium carbonate production both remove DIC from seawater, it is likely that the total quantity of remineralized tDOC is in fact

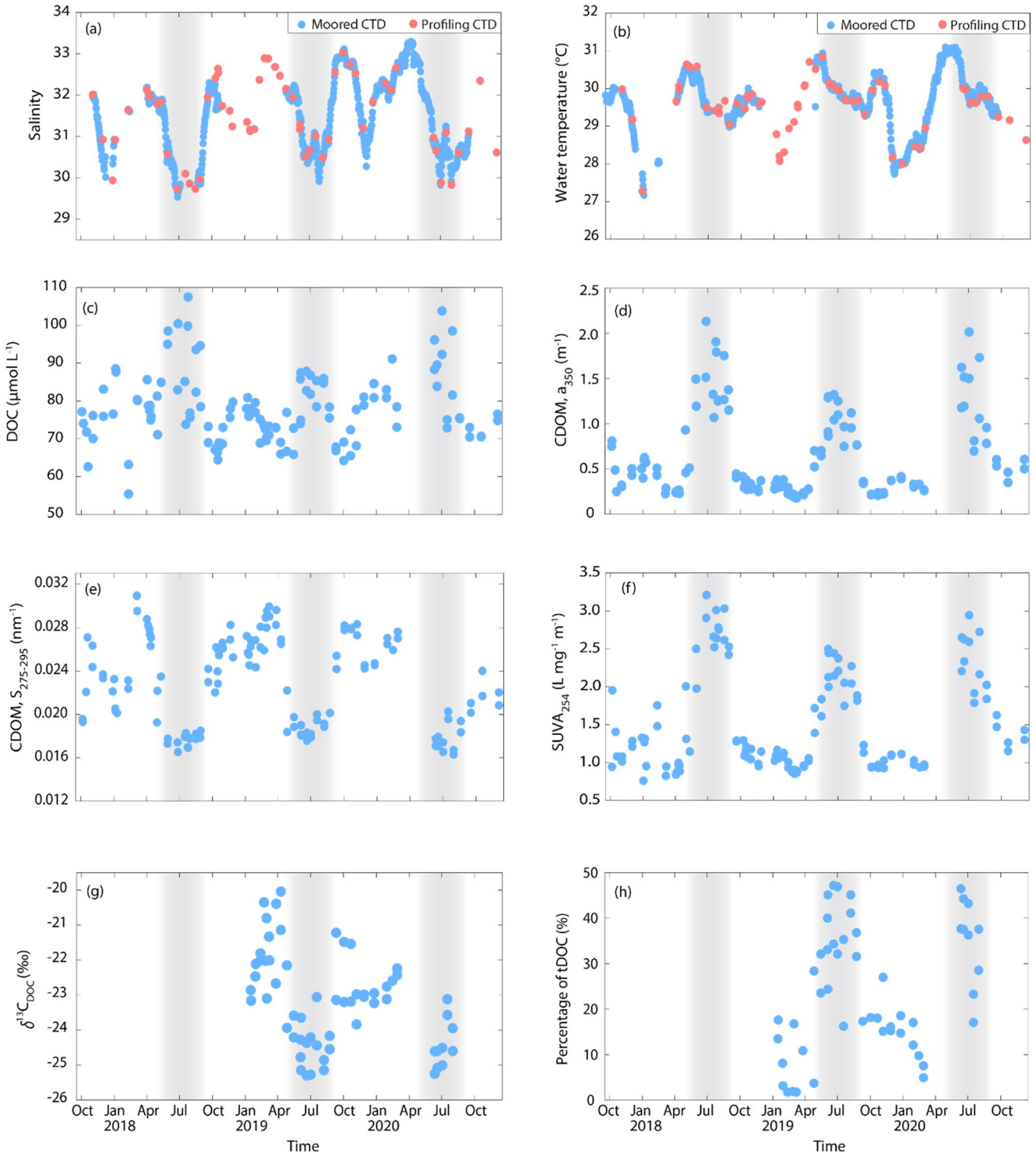

Figure 3. Seasonal variations in biogeochemistry in the Singapore Strait. Time series of (a) salinity, (c) dissolved organic carbon (DOC), (d–f) colored dissolved organic matter (CDOM) and (g) stable isotopic composition ($\delta^{13}C$) of DOC indicates a large input of freshwater and terrigenous dissolved organic matter to our site during the Southwest Monsoon season (May–September, highlighted by gray shading). The water temperature (b) shows small seasonal variation by ~3°C. The salinity and water temperature were both measured by a profiling CTD during each sampling cruise and by a moored CTD. The percentage of terrigenous DOC (tDOC) in the bulk DOC pool (h) was estimated from the $\delta^{13}C_{DOC}$ data.

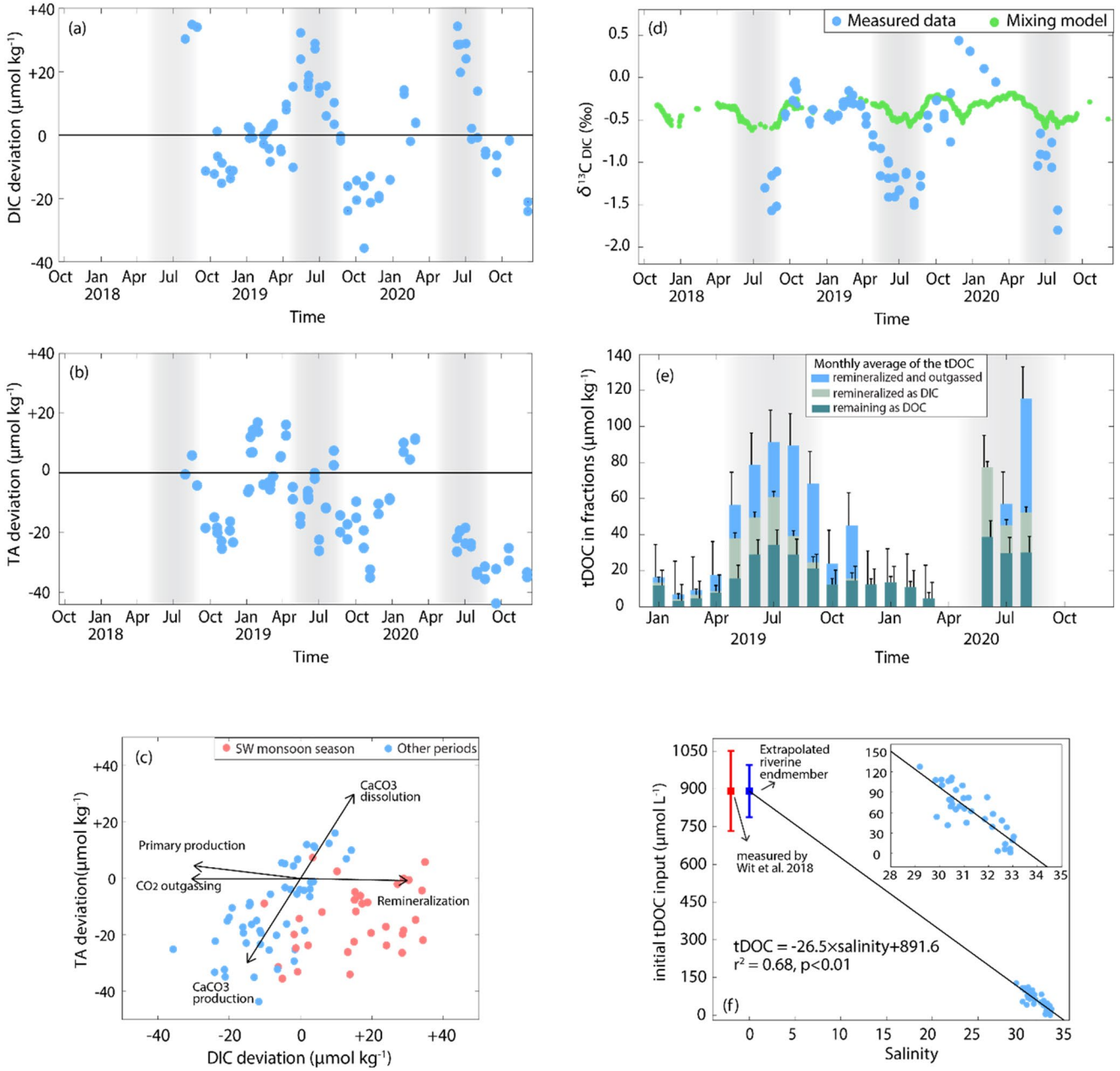

Figure 4. (a and b) Time series of deviations of dissolved inorganic carbon (DIC) and total alkalinity (TA) relative to values expected from the conservative mixing model. DIC shows positive deviation during the Southwest (SW) Monsoon Season (gray shading), coincident with the large tDOC input. (c) Scatterplot of deviation of DIC versus deviation of TA, which indicates a strong signal of remineralization during the SW Monsoon season. (d) The $\delta^{13}C$ of DIC showed strong depletion relative to the mixing model during the SW Monsoon season, indicating remineralization of terrigenous dissolved organic carbon (tDOC). (e) Monthly average quantity of (1) the remaining tDOC, (2) remineralized tDOC that was still present as DIC, (3) remineralized tDOC that had already outgassed to the atmosphere; as estimated by the isotope mass balance calculations. The total height of each stacked bar represents the total initial tDOC concentration in that water before remineralization. The error bars show one standard deviation of each tDOC fraction, as estimated by a Monte Carlo simulation (shown in one direction for clarity). (f) The relationship between salinity and the total initial tDOC concentration yields a predicted peatland riverine endmember DOC concentration of 892 ± 104 μmol L^{-1} (mean ± standard error).

greater than the measured positive deviation of DIC concentration during the SW Monsoon. We therefore turn to $\delta^{13}C_{DIC}$ to estimate the total amount of tDOC remineralization.

The $\delta^{13}C_{DIC}$ in the inter-monsoon seasons varied between −0.4 and 0‰. It decreased to between −1.0 and −1.8‰ during the SW Monsoon (Figure 4d). However, our conservative mixing model predicts that $\delta^{13}C_{DIC}$

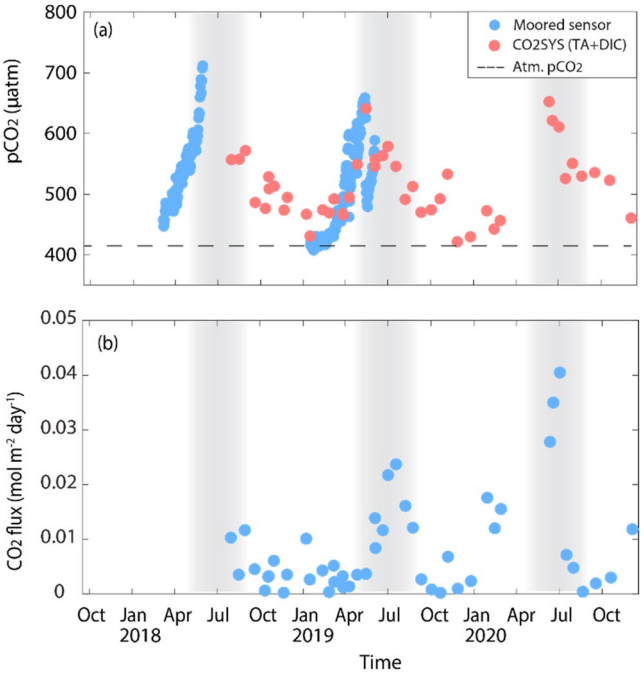

Figure 5. Time series of (a) pCO_2 and the (b) daily areal CO_2 flux. The pCO_2 was measured by a moored SAMI pCO_2 sensor and was validated by the laboratory analysis of total alkalinity (TA) and dissolved inorganic carbon (DIC) using CO2SYS. The data from the latter approach were used for calculation of the CO_2 flux. The Southwest Monsoon season is highlighted by the gray shading.

would vary by only 0.3‰ as a result of riverine DIC input (Figure 4d). This small predicted range is a result of the low DIC concentration in peat-draining, low-pH rivers. The remaining 0.7–1.5‰ decrease in the $\delta^{13}C_{DIC}$ therefore indicates production of extra DIC from an isotopically depleted carbon source, consistent with the remineralization of tDOC within the shelf waters.

3.3. Quantification of tDOC Remineralization by Isotope Mass Balance Calculations

The isotope mass balance calculations provide a breakdown of tDOC remineralization into three fractions (see Section 2.4.2). We assumed that all remineralized terrigenous carbon is derived from tDOC, that is, that terrigenous POC does not contribute to the signals we observe, and that production and remineralization of autochthonous (i.e., marine) DOC are approximately in steady state and do not vary seasonally. The validity of these assumptions is discussed in Section 4.1.

Our SW Monsoon data (Figure 4e) show that the initial total tDOC concentration (represented by the total height of each stacked bar) amounted to between 60 and 140 µmol kg^{-1}. Of this initial tDOC, 20–40 µmol kg^{-1}, or 30%–40%, was still present as unremineralized tDOC at our site, while the remaining 60%–70% had been remineralized in the shelf sea before reaching our site. Of this remineralized tDOC, 10–40 µmol kg^{-1} was still present in the DIC pool, while 15–80 µmol kg^{-1} had been lost to the atmosphere. The proportion of remineralized tDOC that had been removed by outgassing increased over the course of the SW Monsoon. The uncertainty of each carbon fraction ranged from 5–15 µmol kg^{-1} as estimated by a Monte Carlo simulation, indicating an overall quite well-constrained tDOC budget.

The initial total tDOC concentration showed a strong linear relationship with salinity ($[DOC] = -26.5 \times salinity + 891.6$, $r^2 = 0.68$, $p < 0.01$, Figure 4f), the intercept of which implies an average riverine endmember DOC concentration of 892 ± 104 µmol L^{-1} (mean ± standard error). This value is in remarkably close agreement with the reported discharge-weighted mean DOC concentration of Sumatra's main peat-draining rivers, which is 890 ± 159 µmol L^{-1} (Wit et al., 2018), and is too high to be explained by non-peatland tDOC sources.

3.4. Seasonal Variation of Seawater pCO_2 and the Sea-Air CO_2 Flux

The pCO_2 in the Singapore Strait showed oversaturation throughout the year, as well as pronounced seasonal variation. During the inter-monsoon season, pCO_2 was below 500 µatm, but it increased to 550–700 µatm during the SW Monsoon (Figure 5a), consistent with remineralization of tDOC having occurred prior to reaching the Singapore Strait. The high pCO_2 values during the SW Monsoon translated to a daily areal sea-to-air CO_2 flux of 0–41 mmol day^{-1} m^{-2} (Figure 5b). The uncertainty of the CO_2 flux ranges between ±0.1 and ± 8.6 mmol day^{-1} m^{-2} (Data Set S1). The annual areal sea-to-air CO_2 flux in the Singapore Strait, amounted to 2.44 ± 0.17 mol m^{-2} yr^{-1} in 2019 and 4.88 ± 0.47 mol m^{-2} yr^{-1} in 2020.

3.5. Seasonal Acidification and Putative Anthropogenic Contribution

Seawater pH in the Singapore Strait was 7.95–8.03 during the NE Monsoon and the inter-monsoon seasons, when terrestrial input was minor. The pH decreased by up to 0.14, to 7.90–7.85, during the SW Monsoon (Figure 6a, Figure S2b). This pH decrease could be driven by freshwater input, calcium carbonate production, and/or remineralization of organic carbon. Our conservative mixing model only predicts decreases in

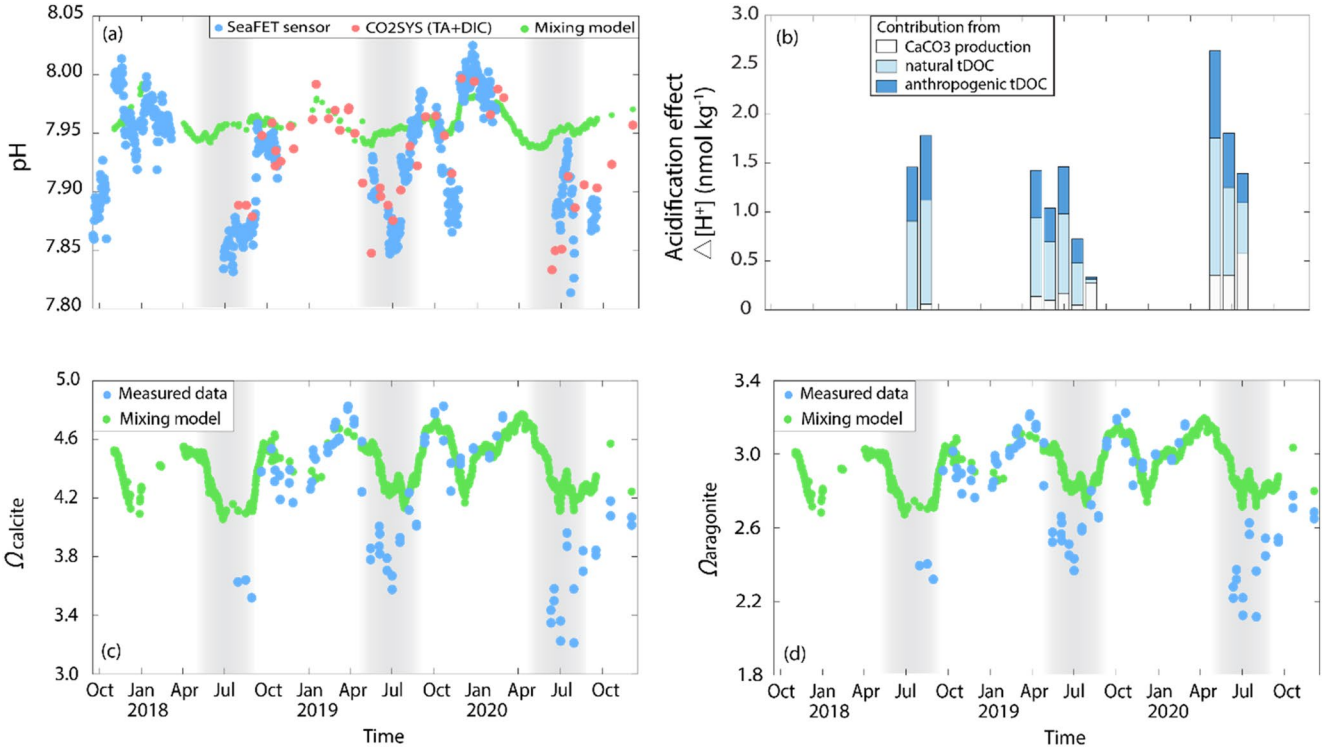

Figure 6. Seasonal acidification during the Southwest (SW) Monsoon season (gray shading) due to the extensive remineralization of terrigenous dissolved organic carbon (tDOC). (a) Time series of pH from the SeaFET sensor and laboratory measurements of total alkalinity (TA) and dissolved inorganic carbon (DIC) shows reduced pH relative to values expected from conservative mixing during the SW Monsoon. (b) Individual contribution to the seasonal acidification from $CaCO_3$ production, remineralization of natural, pre-anthropogenic tDOC, and remineralization of the putative anthropogenic tDOC fraction, based on the results from the mass balance calculations and the reported anthropogenic increase in tDOC export from peatlands (Moore et al., 2013; Yupi et al., 2016). The total acidification effect (height of the stacked bars) is the difference between the measured free proton concentration (calculated from pH) and the predicted value from the conservative mixing model. The results are presented as monthly averages for clarity. (c and d) The saturation states of calcite and of aragonite show large decreases compared to the conservative mixing model during the SW Monsoon season.

seawater pH at our site of ~0.02, indicating that input of river water can only explain a small proportion of this variation (Figure 6a).

We quantified the contribution from calcium carbonate production, natural and anthropogenic tDOC flux and remineralization to the seasonal acidification, expressed as the difference in free proton concentration relative to the conservative mixing ($\Delta[H^+]$, as recommended by Fassbender et al., 2021, Figure). The contribution from calcium carbonate production was only responsible for a small acidification effect, mostly <0.5 nmol kg^{-1} increase in $[H^+]$. The remineralization of tDOC results in 1.0–2.5 nmol kg^{-1} increase in $[H^+]$, accounting for the majority of the seasonal acidification. Assuming that 35% of the total tDOC input during the SW Monsoon, and hence also 35% of the tDOC remineralization, might be an anthropogenic contribution caused by peatland disturbance (Moore et al., 2013; Yupi et al., 2016), we further estimate that 0.3–0.9 nmol kg^{-1} increase in $[H^+]$ of the total acidification effect, or ~35% of the total acidification effect, could be anthropogenic (Figure 6b).

This seasonal variation in the carbonate system also entails changes in the saturation state of calcite (Ω_{CA}) and aragonite (Ω_{AR}). During the late NE Monsoon and inter-monsoon, Ω_{CA} and Ω_{AR} were 4.62 ± 0.09 and 3.07 ± 0.06, respectively (Figure 6c). During the SW Monsoon, the Ω_{CA} decreased to 3.2–4.0 and the Ω_{AR} decreased to 2.1–2.7. These decreases exceeded the decreases predicted by the conservative mixing model by a factor of ≥2.

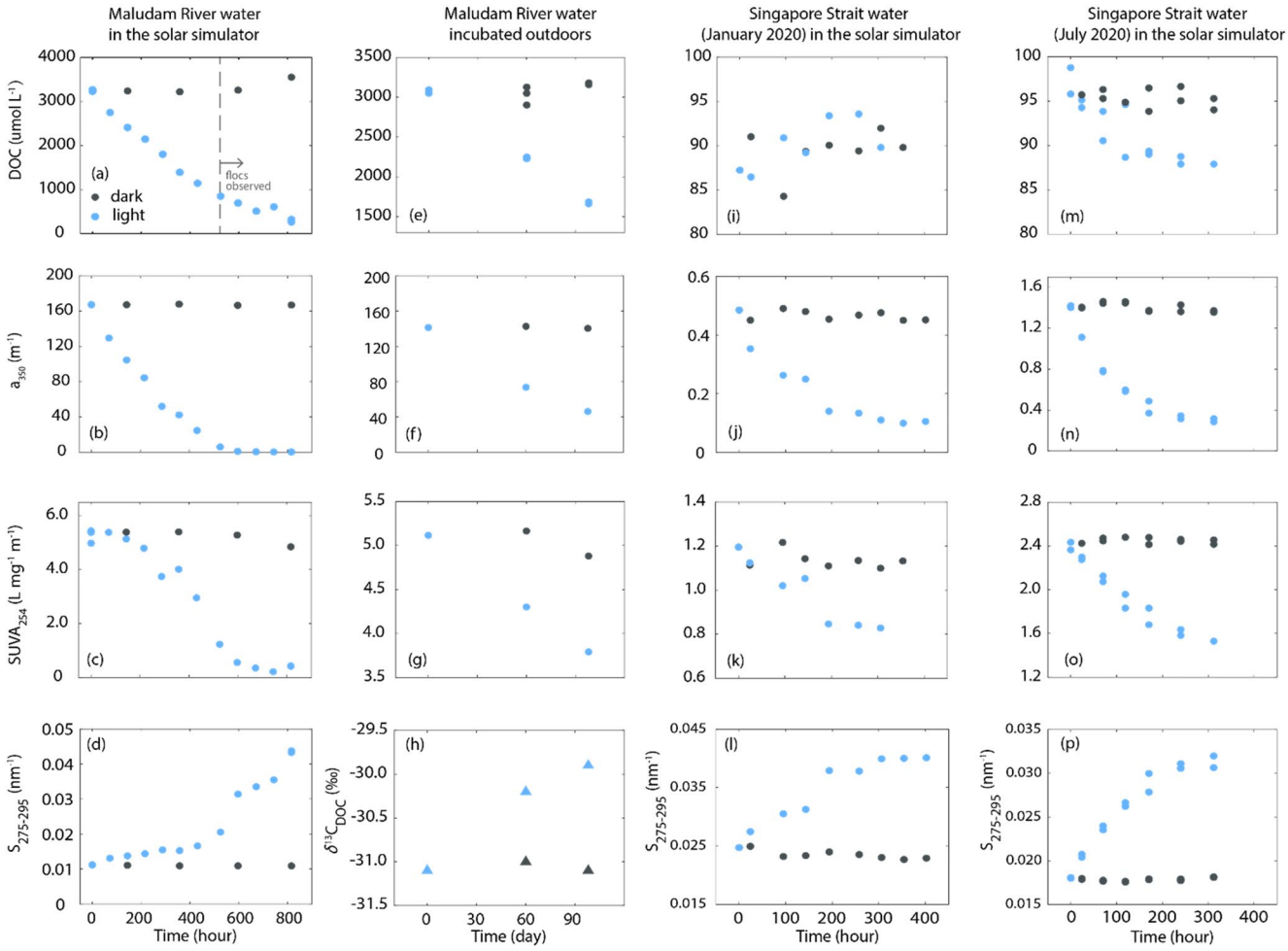

Figure 7. Changes in dissolved organic carbon (DOC), colored dissolved organic matter, and $\delta^{13}C_{DOC}$ during four photodegradation experiments showing high photo-lability of DOC from the Maludam River but only limited photo-lability from the Singapore Strait. Flocs were observed in the water sample after incubation for 525 h during the experiment with the Maludam River water in the solar simulator but were not observed in other experiments.

3.6. Degradability of the Peatland-Derived tDOC

The tDOC from the peatland-draining Maludam River showed high photo-lability (Figure 7, Table 3): the DOC concentration decreased first from 3,250 μmol L^{-1} to 850 μmol L^{-1} over the course of 525 h in the solar simulator (Figure 7a), after which we observed pronounced photo-induced flocculation in the remaining replicates. It is therefore unclear how much of the additional DOC loss after 525 h was due to photo-remineralization. Although POC was not measured, the quantity of flocs did not visibly decrease during the remaining hours of the experiment, suggesting that photo-flocculated DOC probably remained stable. CDOM a_{350} decreased from 167.4 to 5.9 m^{-1}, and the decrease in $SUVA_{254}$ and increase in $S_{275–295}$ indicated the preferential loss of aromatic and high-molecular-weight compounds (Helms et al., 2008; Weishaar et al., 2003) (Figures 7b–7d). The decrease in DOC up to 525 h (before we observed flocs) implies that around 74% of tDOC was labile to photochemical remineralization.

The experiment in which Maludam River water was exposed to natural sunlight revealed that photodegradation also resulted in a modest isotopic fractionation (Figures 7e–7h, Table 3). The DOC concentration decreased by 45% from 3,069 to 1,674 μmol L^{-1}, and $\delta^{13}C_{DOC}$ increased from −31.1 to −29.9‰. This implies that the resulting DIC had a $\delta^{13}C$ value of −32.5‰, and that photodegradation of this tDOC therefore entailed a fractionation of −1.4‰. As in the previous experiment, CDOM and $SUVA_{254}$ decreased strongly, while $S_{275–295}$ increased.

Table 3
Results of the Photodegradation Experiments

	DOC (μmol L^{-1})	a_{350} (m^{-1})	$S_{275-295}$ (nm^{-1})	$SUVA_{254}$ (L mg^{-1} m^{-1})	$\delta^{13}C_{DOC}$ (‰)	$\delta^{13}C_{DIC}$[a] (‰)
Maludam River in solar simulator[b]						
Before	3,250	167.4	0.011	5.41		
After	850	5.9	0.021	1.23		
%loss	74%	96%				
Maludam River incubated outdoors						
Before	3,069	140.88	0.012	5.12	−31.1	-
After	1,674	46.41	0.015	3.79	−29.9	−32.5
%loss	45%	67%				
Singapore Strait, NE Monsoon (January 2020)						
Before	87	0.49	0.025	1.20		
After	89	0.11	0.040	0.83		
%loss	-	78%				
Singapore Strait, SW Monsoon (July 2020)						
Before	97	1.40	0.018	2.40		
After	88	0.29	0.032	1.53		
%loss	9%	79%				

Abbreviations: DIC, dissolved inorganic carbon; DOC, dissolved organic carbon; NE, Northeast; SW, Southwest; TA, total alkalinity.
[a]$\delta^{13}C$ of the DIC produced from remineralization of the initial DOC. [b]Data beyond 525 h were omitted because flocculation observed.

Samples collected from the Singapore Strait during the NE (Figures 7i–7l) and SW Monsoon (Figures 7m–7p) both showed pronounced losses of CDOM upon experimental irradiation for >300 h, but at most small losses of DOC. There was a decrease in a_{350} by >70%, and strong decreases in $SUVA_{254}$ and increases in $S_{275-295}$ during both seasons. However, the NE Monsoon sample showed no change in DOC concentration (Figure 7i); the SW Monsoon sample only showed a decrease in DOC concentration by 9 μmol L^{-1} (Figure 7m). Of the bulk DOC in this SW Monsoon sample, 36 μmol L^{-1} was tDOC (estimated from the $\delta^{13}C_{DOC}$). Because the majority of the DOC pool during the NE Monsoon is of marine origin, it appears that the autochthonous marine DOC is not strongly photolabile. Assuming therefore that the observed decrease in DOC in the SW Monsoon experiment was entirely due to tDOC remineralization, our results would indicate that only about 25% (9 out of 36 μmol L^{-1}) of the peatland-derived tDOC that still remains in organic form in the Singapore Strait is labile to direct photochemical remineralization.

Moreover, we found that the biodegradability of the SW Monsoon sample from the Singapore Strait was low, with <6% loss of DOC and CDOM a_{350} over the course of the 109-day incubation (Figure 8). Although the leucine and glucose added as labile carbon to one treatment was rapidly consumed, no additional remineralization of DOC was induced in this treatment. Our results, consistent with the low biodegradability of tDOC from the Maludam River (Nichols & Martin, 2021), suggest that direct microbial remineralization is not a main driver of tDOC remineralization. Whether the observed biodegradation represents loss of tDOC at all or only of autochthonous DOC is unclear.

In summary, our experiments with the Maludam River samples indicate that around 74% of tDOC is directly photo-remineralizable, while our observational data from the Singapore Strait show that 60%–70% of the peatland-derived tDOC is remineralized in the coastal waters of the Sunda Shelf. Our additional experiments then show that of the remaining 30%–40% of this tDOC, <25% is still photo-remineralizable, which means that at most additional remineralization of 7%–10% of the initial tDOC flux might occur during its transport from the Singapore Strait to the exits of the shelf to the open ocean, and that any biodegradation proceeds at most slowly. Depending on how much of the remaining tDOC really is biodegradable, these results imply that possibly around 20%–30% of the total peatland tDOC from Sumatra is sufficiently refractory to resist remineralization on the Sunda Shelf and be exported to the Indian Ocean, given that the total water residence time in the Malacca Strait is approximately 2 years (Mayer et al., 2018).

4. Discussion

4.1. Sources of tDOC

The correlated seasonal variations of salinity, DOC, $\delta^{13}C_{DOC}$, CDOM absorption, and spectral characteristics all indicate that our site receives a large input of tDOC during the SW Monsoon, and a much smaller tDOC input during the NE Monsoon. The high riverine endmember DOC concentration (892 ± 104 μmol L^{-1}) predicted from the relationship between the total initial tDOC concentration and salinity (Figure 4f) clearly points to peatlands as the source of the tDOC measured during the SW Monsoon. This seasonally variable advection of peatland tDOC explains the lack of a strong peatland signal in the carbonate system data measured by Hamzah et al. (2020) in the Karimata Strait to the southeast of our site: because they sampled during the SW Monsoon, the peatland-influenced water would have flowed northwards away from their transect and out to the South China Sea. It should be noted that the seasonality in our data are primarily the result of seasonal changes in ocean currents, and not primarily because of seasonal changes in peatland tDOC delivery. Although seasonal variation in rainfall can cause variation in tDOC flux from tropical peatlands (Rixen et al., 2016), peatland-influenced coastal waters in Southeast Asia receive relatively high

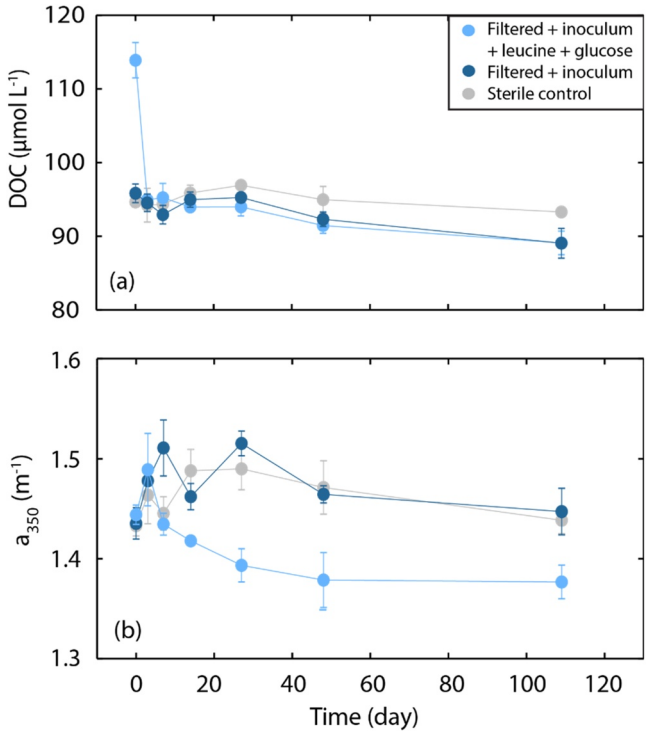

Figure 8. Changes in (a) dissolved organic carbon (DOC) and (b) colored dissolved organic matter (a_{350}) during the 109-day incubation showing limited biodegradability of DOC collected from the Singapore Strait.

tDOC inputs year-round (Martin et al., 2018; Wit et al., 2015, 2018; Zhou et al., 2019).

Our isotope mass balance calculations assume that the seasonal variation in our data is not driven by seasonal changes in autochthonous DOC remineralization. The relatively low chlorophyll-*a* concentrations year-round suggest that autochthonous organic matter production rates are moderate and, importantly, do not show strong seasonality. This is likely due to persistent light limitation caused by strong vertical light attenuation (Chow et al., 2019; Martin et al., in press; Morgan et al., 2020) and tidal mixing of the water column, which prevents vertical stratification (Mayer & Pohlmann, 2014). Moreover, the very small annual range in seawater temperature means that microbial physiological rates will not vary strongly. Therefore, the net community production rate is most likely relatively constant, and we can rule out the possibility that our observations are the result of seasonal changes in production and remineralization of marine autochthonous organic matter. Moreover, the seasonal decrease in $\delta^{13}C_{DIC}$ is too large to be explained by the remineralization of marine DOC with a $\delta^{13}C_{DOC}$ of around −22‰. Even though we attributed all the excess DIC to remineralization of tDOC with $\delta^{13}C$ of DIC production of −32‰, the depletion in $\delta^{13}C_{DIC}$ was so large that it could only be explained by inferring that an even greater quantity of tDOC had been remineralized and outgassed.

We further assume that the remineralized terrigenous carbon is tDOC rather than POC. The terrigenous organic carbon in peat-draining rivers in Southeast Asia is overwhelmingly in form of DOC year-round (typically ≥95%) (Alkhatib et al., 2007; Baum et al., 2007; Moore et al., 2011; Müller et al., 2015), and thus any terrigenous POC input is expected to be small in this region. Part of any POC that is delivered by rivers is also likely to sink and accumulate in the sediment, thus decoupling the POC and its remineralization from the water carrying the DOC. Most importantly, the riverine endmember DOC concentration that we infer from our regression of total initial tDOC concentrations versus salinity (892 ± 104 μmol L^{-1}) is also very close to the discharge-weighted average DOC concentration measured independently in the main peatland-draining rivers on Sumatra, of 890 ± 159 μmol L^{-1} (Wit et al., 2018). This indicates that additional remineralization of POC is not required to explain the observed variation in DIC and $\delta^{13}C_{DIC}$.

4.2. Remineralization of tDOC

Remineralization of tDOC can occur either by microbial decomposition (i.e., biodegradation) or by photochemical decomposition. Biodegradation is increasingly recognized as an important pathway of tDOC decomposition in aquatic systems (Tranvik et al., 2009; N. D. Ward et al., 2013; Wickland et al., 2007). However, peatland organic matter especially in the tropics is enriched in polyphenolic compounds such as lignin derivatives, which are likely refractory to microbial respiration (Gandois et al., 2014; Hodgkins et al., 2018). Our data showed at most low biodegradability of the tDOC collected from the Singapore Strait, even when amended with labile carbon to stimulate a potential priming effect (Bianchi, 2011; Guenet et al., 2010; van Nugteren et al., 2009). Similarly, freshly collected tDOC from the peatland-draining Maludam River showed at most very limited biodegradability over 56 days, even when amended with dissolved nutrients or mixed into coastal seawater (Nichols & Martin, 2021). In contrast, we found that up to about 74% of peatland-derived tDOC can be photochemically remineralized. This is consistent with previous reports of high photo-lability of tropical peatland tDOC (Gandois et al., 2020; Martin et al., 2018; Spencer et al., 2009). Collectively, these results suggest that photodegradation rather than biodegradation likely drives the observed remineralization.

It is possible that partial photodegradation increases the biodegradability of the peatland tDOC (Cory & Kling, 2018; Moran & Zepp, 1997; Moran et al., 2000). For example, tDOC processing in Arctic freshwater systems depends on initial photodegradation that stimulates subsequent microbial remineralization (Cory et al., 2014), and 32% of the tDOC remineralization on the Louisiana Shelf was attributed to photochemically stimulated biodegradation (Fichot & Benner, 2014). Our experimental data are consistent with preferential degradation of high-molecular-weight aromatic substances during irradiation, which is believed to increase tDOC biodegradability, although it should be noted that photodegradation can also compete with microbial degradation of tDOC (C. P. Ward et al., 2017). Further studies are required to address the importance of photochemical-microbial interactions for Southeast Asian peatland tDOC decomposition.

4.3. CO_2 Emissions From the Sunda Shelf Driven by tDOC Remineralization

The mass balance calculations showed that the proportion of the remineralized tDOC that had been removed by CO_2 outgassing increased throughout the SW Monsoon, indicating the ongoing removal of CO_2 to atmosphere. Our estimate that the Singapore Strait contributes a net sea-to-air CO_2 flux of 2.44–4.88 mol m^{-2} yr^{-1} is consistent with the paradigm that tropical inner shelves tend to act as sources of atmospheric CO_2 (Cai, 2011; Chen & Borges, 2009; Chen et al., 2013). Our estimate is comparable to that of Wit et al. (2018) for the same region (4.12 mol m^{-2} yr^{-1}), but is much higher than the estimates by Roobaert et al. (2019) (0–0.4 mol m^{-2} yr^{-1}) and Hamzah et al. (2020) (1.09 mol m^{-2} yr^{-1}). The estimates of Roobaert et al. (2019) were based on a global data product that lacked direct measurements from the Sunda Shelf Sea, while Hamzah et al. (2020) sampled in the southern Karimata Strait during the SW Monsoon, at which point the peatland tDOC is advected northeastwards into the South China Sea. The fact that the Sunda Shelf is clearly a stronger CO_2 source than estimated by some studies demonstrates the importance of collecting annual time series of carbon biogeochemistry in this region, and of increasing the data coverage for coastal waters in Southeast Asia.

Since 90% of Southeast Asia's peatlands have experienced anthropogenic disturbance (Miettinen et al., 2016), it is likely that the tDOC input to the Sunda Shelf is at present significantly elevated relative to historical values. Given that the extent of tDOC remineralization that we infer within the shelf is close to our experimental measurements of tDOC decomposability from an intact peatland catchment (the Maludam River), our data indicate that the majority of any anthropogenically mobilized peatland tDOC must be largely remineralized within the shelf sea, and then outgassed to the atmosphere. This is consistent with existing recommendations for estimating downstream anthropogenic CO_2 emissions from peatland DOC remineralization (Evans et al., 2016; IPCC, 2014), although our results suggest that the extent of peatland tDOC remineralization (at least over the residence time of the Sunda Shelf) might be slightly lower than the value of 90% that is currently used for peatland emissions reporting (IPCC, 2014). Overall, however, our study clearly highlights the importance of downstream greenhouse gas emissions from tropical peatland disturbance, and suggests that increased peatland tDOC input results in increased tDOC remineralization and CO_2 outgassing from the shelf sea.

4.4. Seasonal Acidification Driven by tDOC Remineralization

During the SW Monsoon, 10–30 μmol kg^{-1} of the remineralized tDOC is still present as DIC upon reaching the Singapore Strait, resulting in a seasonal pH decline by 0.06–0.10 and a large decrease in the saturation state of $CaCO_3$. The potential role of tDOC remineralization as a driver of shelf sea acidification has so far received limited attention, but was recently shown to be important in the Arctic Ocean (Capelle et al., 2020; Semiletov et al., 2016). A large impact of tDOC remineralization on the carbonate system was reported in the estuaries and coastal waters of eastern Sumatra (Wit et al., 2018). Our results further show that the seasonal advection of these waters subjects sensitive calcifying communities such as coral reefs, which are found further away from the peatland river estuaries around the islands to the east of Sumatra (UNEP-WCMC, 2010), to pronounced seasonal acidification.

A decrease in the saturation state (Ω) of calcium carbonate and can impair the growth of corals by reducing calcification rates (Cooper et al., 2008; Langdon, 2005; Pisapia et al., 2019) and skeletal density (Manzello et al., 2008; Mollica et al., 2018), and can contribute to the degradation of coral reefs by promoting coral

bleaching (Anthony et al., 2008; DeCarlo et al., 2017; Fabricius et al., 2011) and decreases in coral species diversity (Fabricius et al., 2011). Specifically, net carbonate loss on coral reefs might be induced when the Ω_{AR} decreases to ~3.3 or below (Hoegh-Guldberg et al., 2007; Kleypas et al., 1999), and large-scale reductions in calcification have been projected for future high-pCO_2 scenarios due to anthropogenic CO_2 emissions (Andersson et al., 2007; Anthony et al., 2008; Dove et al., 2013; Hoegh-Guldberg et al., 2007). The decrease in Ω_{AR} to ~2.7 at our site during the SW Monsoon might therefore reduce coral calcification and reef development during this period of the year, as has been shown in response to seasonal carbonate system variation in the Great Barrier Reef (Dove et al., 2013; Stoltenberg et al., 2021).

Recent surveys indicate that many coral reefs in the coastal ocean of Sumatra show fair or poor status, likely due to a combination of stressors (Cinner et al., 2016; Hadi et al., 2020). Our data show that acidification driven by tDOC remineralization is potentially one important stressor for reefs in this region. While such tDOC-driven acidification can be off-set by marine primary production in shelf seas that are sufficiently productive (Capelle et al., 2020), low productivity due to nutrient limitation might make oligotrophic tropical waters more vulnerable to such additional inputs of CO_2. Furthermore, we find that the reported increases in tDOC flux after peatland disturbance (Moore et al., 2013; Yupi et al., 2016) are sufficiently large to account for a significant part of the observed acidification. This anthropogenic acidification source needs to be recognized more alongside other anthropogenic impacts on coastal seawater pH dynamics, such as eutrophication (Cai et al., 2011; Duarte et al., 2013; Melzner et al., 2013). Importantly, tDOC remineralization is independent of the ocean acidification caused by dissolution of the increasing atmospheric CO_2 since the industrial era. As rising atmospheric CO_2 will progressively lower the pH and buffer capacity of seawater entering the Sunda Shelf from the South China Sea in future, remineralization of tDOC will then lead to even larger pH decreases than in the present (Pacella et al., 2018).

4.5. Implications for the Fate of tDOC in the Ocean

Our results suggest that the Sunda Shelf Sea contributes to the remineralization and outgassing of a significant fraction of the global land–ocean tDOC flux, and is likely a more efficient filter for tDOC compared to other shelf seas. For example, the Amazon River delivers a comparable amount of tDOC to the ocean (15%–20% of the global tDOC flux), but the fast transport across the relatively narrow shelf area results in a water residence time <2 months (Coles et al., 2013) and allows 50%–76% of tDOC to be delivered to the open Atlantic Ocean (Medeiros et al., 2015). The larger area (1,893,307 km^2) and much longer water residence time (~2 years) of the Sunda Shelf Sea (Mayer et al., 2015) clearly allow for more extensive tDOC remineralization within the shelf. In addition, the coastal location of Southeast Asia's peatlands reduces the residence time of tDOC within the freshwater system and therefore the potential for part of the tDOC to be remineralized before reaching the shelf sea (Wit et al., 2015). In contrast, respiration within the Amazon river helps to remove the more labile tDOC fractions already before reaching the shelf (N. D. Ward et al., 2013), which potentially explains why tDOM was found to be relatively stable in the Amazon River plume (Medeiros et al., 2015). The world's second largest river, the Congo River, also drains a large area of tropical peatlands located in the central Congo Basin (Dargie et al., 2017). Previous work has reported high photo-lability of tDOC from the Congo River (Spencer et al., 2009; Stubbins et al., 2010) and Aarnos et al. (2018) estimated that 30% of Congo River tDOC is photochemically remineralized, but that most of this photodegradation takes place beyond the narrow shelf sea in the open Atlantic Ocean. At mid- and high latitudes, estimates of shelf sea tDOC remineralization are typically lower than our estimate for the Sunda Shelf: 40% tDOC remineralization was reported for the Louisiana Shelf (Fichot & Benner, 2014), and 50%–56% on the Eurasian Shelf of the Arctic Ocean (Kaiser et al., 2017; Letscher et al., 2011), although Fransner et al. (2018) inferred that 80% of tDOC entering the Gulf of Bothnia might be labile over a timescale of 1 year. Based on experimental data from 10 of the world's major rivers, Aarnos et al. (2018) estimated that around 70% of global tDOC flux to the ocean is remineralized within 1 year, both on and beyond shelf seas.

Our results are comparable to a recent estimate that 63% of the total peatland carbon lost to rivers in Southeast Asia is remineralized, which was derived by scaling up sea-to-air CO_2 fluxes in the southern Malacca Strait and Karimata Strait (Wit et al., 2018). That study further assumed that essentially all of the remaining tDOC would be remineralized subsequently in the surface ocean. However, our incubations showed surprisingly low lability of the remaining tDOC by both microbial and photochemical decomposition, even

though most of the CDOM was lost due to photobleaching. Consequently, our data suggest that it is possible that roughly 20%–30% of the tDOC from Sumatran peatlands (and likely also from the similarly extensive peatlands on Borneo) is actually exported to the open Indian Ocean (see Section 3.6) and might ultimately contribute to the semi-refractory or even refractory oceanic DOC pool. This is consistent with the hypothesis that tDOC might actually contribute a larger share of the global oceanic DOC pool than previously believed, which was recently suggested based on isotopic (Follett et al., 2014; Zigah et al., 2017) and molecular analyses of marine DOC samples (Cao et al., 2018; Medeiros et al., 2016). While our data thus confirm that the Sunda Shelf is a particularly efficient site for tDOC remineralization, they nevertheless leave open the possibility that Southeast Asia might provide an important input of tDOC to the oceanic DOC pool.

5. Conclusions

Our results demonstrate that the large input of tDOC from peatlands on Sumatra significantly affects regional DOC concentrations, CO_2 fluxes, and the carbonate system in the Sunda Shelf Sea. Isotope mass balance calculations indicate that 60%–70% of this tDOC is remineralized in the coastal waters of the shelf sea close to the peatlands, and incubation experiments suggest that photodegradation drives a significant part of this remineralization. The increase in DIC concentration caused by this remineralization results in a seasonal decrease in seawater pH by up to 0.10, of which the remineralization of the putative anthropogenic tDOC fraction might account for 35% of the total proton addition, potentially impacting coral physiology in the region. Most of the CO_2 produced from this tDOC remineralization is likely eventually lost to the atmosphere. Our data thus provide evidence that there is a large indirect pathway of CO_2 emissions to the atmosphere due to peatland disturbance via the remineralization of tDOC in coastal seas. Despite this rapid remineralization of a large fraction of tDOC, we also found low bio- and photo-degradability of the residual tDOC pool. We conclude that the Sunda Shelf is an efficient sink of peatland-derived tDOC and a significant source of atmospheric CO_2, but that a higher proportion of the peatland tDOC might be refractory and exported to the Indian Ocean than was previously thought. The long-term fate of this tDOC flux to the open ocean remains uncertain.

Conflict of Interest

The authors declare no conflicts of interest relevant to this study.

Data Availability Statement

All processed data are available in the Supplementary Data Table. All raw data files and analysis codes are available through the Nanyang Technological University Data Repository (https://doi.org/10.21979/N9/HK8M00).

Acknowledgments
The authors thank Molly Moynihan, Nikita Kaushal, Robert Nichols, Ashleen Tan Su Ying, Chen Shuang, Woo Oon Yee, Kyle Morgan, and Phyllis Kho Yu Yi for help during field work and laboratory analysis. The authors are very grateful to Nikita Kaushal for measuring $\delta^{13}C_{DIC}$, to Nathalie Goodkin for providing the moored CTD and pH sensors for this work, to Evelyn Lim for performing some of the photodegradation experiments, to Moritz Müller for collecting water samples from the Maludam River, and to Francis Yeo, Sapari, and Surpato of *Dolphin Explorer* for enabling the sample collection. The contribution of CDE was supported by the UK Natural Environment Research Council's LOCATE project, NE/N018087/1. The authors thank the two anonymous reviewers for their constructive comments. Our work was carried out with the permission of the National Parks Board, Singapore (research permit No. NP/RP17-044-3). This research was funded by the National Research Foundation Singapore, Prime Minister's Office, as part of the Marine Science Research and Development Programme through grant MSRDP-P32 to Patrick Martin, and forms part of the Ph.D. research of Yongli Zhou.

References

Aarnos, H., Gélinas, Y., Kasurinen, V., Gu, Y., Puupponen, V. M., & Vähätalo, A. V. (2018). Photochemical mineralization of terrigenous DOC to dissolved inorganic carbon in ocean. *Global Biogeochemical Cycles*, *32*(2), 250–266. https://doi.org/10.1002/2017GB005698

Alkhatib, M., Jennerjahn, T. C., & Samiaji, J. (2007). Biogeochemistry of the Dumai River estuary, Sumatra, Indonesia, a tropical blackwater river. *Limnology and Oceanography*, *52*(6), 2410–2417. https://doi.org/10.4319/lo.2007.52.6.2410

Alling, V., Humborg, C., Mörth, C.-M., Rahm, L., & Pollehne, F. (2008). Tracing terrestrial organic matter by $d^{34}S$ and $d^{13}C$ signatures in a subarctic estuary. *Limnology and Oceanography*, *53*(6), 2594–2602. https://doi.org/10.4319/lo.2008.53.6.2594

Andersson, A. J., Bates, N. R., & Mackenzie, F. T. (2007). Dissolution of carbonate sediments under rising pCO_2 and ocean acidification: Observations from Devil's Hole, Bermuda. *Aquatic Geochemistry*, *13*(3), 237–264. https://doi.org/10.1007/s10498-007-9018-8

Anthony, K. R. N., Kline, D. I., Diaz-Pulido, G., Dove, S., & Hoegh-Guldberg, O. (2008). Ocean acidification causes bleaching and productivity loss in coral reef builders. *Proceedings of the National Academy of Sciences of the United States of America*, *105*(45), 17442–17446. https://doi.org/10.1073/pnas.0804478105

Assayag, N., Rivé, K., Ader, M., Jézéquel, D., & Agrinier, P. (2006). Improved method for isotopic and quantitative analysis of dissolved inorganic carbon in natural water samples. *Rapid Communications in Mass Spectrometry*, *20*(15), 2243–2251. https://doi.org/10.1002/rcm.2585

Baum, A. (2008). *Tropical blackwater biogeochemistry : The Siak River in Central Sumatra, Indonesia* (PhD thesis). University of Bremen.

Baum, A., Rixen, T., & Samiaji, J. (2007). Relevance of peat draining rivers in central Sumatra for the riverine input of dissolved organic carbon into the ocean. *Estuarine, Coastal and Shelf Science*, *73*(3–4), 563–570. https://doi.org/10.1016/j.ecss.2007.02.012

Bauman, A. G., Hoey, A. S., Dunshea, G., Feary, D. A., Low, J., & Todd, P. A. (2017). Macroalgal browsing on a heavily degraded, urbanized equatorial reef system. *Scientific Reports*, *7*(1), 1–8. https://doi.org/10.1038/s41598-017-08873-3

Beleites, C., & Sergo, V. (2012). hyperSpec: A package to handle hyperspectral data sets in R. *Journal of Statistical Software*.
Bianchi, T. S. (2011). The role of terrestrially derived organic carbon in the coastal ocean: A changing paradigm and the priming effect. *Proceedings of the National Academy of Sciences of the United States of America*, *108*(49), 19473–19481. https://doi.org/10.1073/pnas.1017982108
Cai, W.-J. (2011). Estuarine and coastal ocean carbon paradox: CO_2 sinks or sites of terrestrial carbon incineration? *Annual Review of Marine Science*, *3*(1), 123–145. https://doi.org/10.1146/annurev-marine-120709-142723
Cai, W.-J., Hu, X., Huang, W.-J., Murrell, M. C., Lehrter, J. C., Lohrenz, S. E., et al. (2011). Acidification of subsurface coastal waters enhanced by eutrophication. *Nature Geoscience*, *4*(11), 766–770. https://doi.org/10.1038/ngeo1297
Cao, X., Aiken, G. R., Butler, K. D., Huntington, T. G., Balch, W. M., Mao, J., & Schmidt-Rohr, K. (2018). Evidence for major input of riverine organic matter into the ocean. *Organic Geochemistry*, *116*, 62–76. https://doi.org/10.1016/j.orggeochem.2017.11.001
Capelle, D. W., Zou, A., Kuzyk, Z., Papakyriakou, T., Guéguen, C., Miller, L. A., & Macdonald, R. W. (2020). Effect of terrestrial organic matter on ocean acidification and CO2 flux in an Arctic Shelf Sea. *Progress in Oceanography*, *185*, 102319. https://doi.org/10.1016/j.pocean.2020.102319
Chen, C.-T. A., & Borges, A. V. (2009). Reconciling opposing views on carbon cycling in the coastal ocean: Continental shelves as sinks and near-shore ecosystems as sources of atmospheric CO_2. *Deep Sea Research Part II: Topical Studies in Oceanography*, *56*(8–10), 578–590. https://doi.org/10.1016/j.dsr2.2009.01.001
Chen, C.-T. A., Huang, T.-H., Chen, Y.-C., Bai, Y., He, X., & Kang, Y. (2013). Air–sea exchanges of CO2 in the world's coastal seas. *Biogeosciences*, *10*(10), 6509–6544. https://doi.org/10.5194/bg-10-6509-2013
Cheng, L., Normandeau, C., Bowden, R., Doucett, R., Gallagher, B., Gillikin, D. P., et al. (2019). An international intercomparison of stable carbon isotope composition measurements of dissolved inorganic carbon in seawater. *Limnology and Oceanography: Methods*, *17*(3), 200–209. https://doi.org/10.1002/lom3.10300
Chow, G. S. E., Chan, Y. K. S., Jain, S. S., & Huang, D. (2019). Light limitation selects for depth generalists in urbanised reef coral communities. *Marine Environmental Research*, *147*, 101–112. https://doi.org/10.1016/j.marenvres.2019.04.010
Chupakova, A. A., Chupakov, A. V., Neverova, N. V., Shirokova, L. S., & Pokrovsky, O. S. (2018). Photodegradation of river dissolved organic matter and trace metals in the largest European Arctic estuary. *Science of the Total Environment*, *622–623*, 1343–1352. https://doi.org/10.1016/j.scitotenv.2017.12.030
Cinner, J. E., Huchery, C., MacNeil, M. A., Graham, N. A. J., McClanahan, T. R., Maina, J., et al. (2016). Bright spots among the world's coral reefs. *Nature*, *535*(7612), 416–419. https://doi.org/10.1038/nature18607
Coles, V. J., Brooks, M. T., Hopkins, J., Stukel, M. R., Yager, P. L., & Hood, R. R. (2013). The pathways and properties of the Amazon river plume in the tropical North Atlantic Ocean. *Journal of Geophysical Research: Oceans*, *118*(12), 6894–6913. https://doi.org/10.1002/2013JC008981
Cooper, T. F., De'ath, G., Fabricius, K. E., & Lough, J. M. (2008). Declining coral calcification in massive Porites in two nearshore regions of the northern Great Barrier Reef. *Global Change Biology*, *14*(3), 529–538. https://doi.org/10.1111/j.1365-2486.2007.01520.x
Cory, R. M., & Kling, G. W. (2018). Interactions between sunlight and microorganisms influence dissolved organic matter degradation along the aquatic continuum. *Limnology and Oceanography Letters*, *3*, 102–116. https://doi.org/10.1002/lol2.10060
Cory, R. M., Ward, C. P., Crump, R. C., & Kling, G. W. (2014). Sunlight controls water column processing of carbon in arctic fresh waters. *Science*, *345*(6199), 925–928.
CYGNSS. (2017). *CYGNSS level 2 science data record version 2.1*. NASA Physical Oceanography DAAC. https://doi.org/10.5067/CYGNS-L2X21
Dargie, G. C., Lewis, S. L., Lawson, I. T., Mitchard, E. T. A., Page, S. E., Bocko, Y. E., & Ifo, S. A. (2017). Age, extent and carbon storage of the central Congo Basin peatland complex. *Nature*, *542*(7639), 86–90. https://doi.org/10.1038/nature21048
DeCarlo, T. M., Cohen, A. L., Wong, G. T. F., Shiah, F.-K., Lentz, S. J., Davis, K. A., et al. (2017). Community production modulates coral reef pH and the sensitivity of ecosystem calcification to ocean acidification. *Journal of Geophysical Research: Oceans*, *122*(1), 745–761. https://doi.org/10.1002/2016JC012326
Dickson, A. G. (1990). Standard potential of the reaction: AgCl(s)+12H2(g)=Ag(s)+HCl(aq), and the standard acidity constant of the ion HSO_4^- in synthetic sea water from 273.15 to 318.15 K. *The Journal of Chemical Thermodynamics*, *22*(2), 113–127. https://doi.org/10.1016/0021-9614(90)90074-Z
Dickson, A. G., & Millero, F. J. (1987). A comparison of the equilibrium constants for the dissociation of carbonic acid in seawater media. *Deep Sea Research Part A: Oceanographic Research Papers*, *34*(10), 1733–1743. https://doi.org/10.1016/0198-0149(87)90021-5
Dlugokencky, E. J., Mund, J. W., Crotwell, A. M., Crotwell, M. J., & Thoning, K. W. (2021). *Atmospheric carbon dioxide dry air mole fractions from the NOAA GML carbon cycle cooperative global air sampling network, 1968–2019, version: 2021-02*. https://doi.org/10.15138/wkgj-f215
Dommain, R., Couwenberg, J., Glaser, P. H., Joosten, H., & Suryadiputra, I. N. N. (2014). Carbon storage and release in Indonesian peatlands since the last deglaciation. *Quaternary Science Reviews*, *97*, 1–32. https://doi.org/10.1016/j.quascirev.2014.05.002
Dove, S. G., Kline, D. I., Pantos, O., Angly, F. E., Tyson, G. W., & Hoegh-Guldberg, O. (2013). Future reef decalcification under a business-as-usual CO_2 emission scenario. *Proceedings of the National Academy of Sciences of the United States of America*, *110*(38), 15342–15347. https://doi.org/10.1073/pnas.1302701110
Duarte, C. M., Hendriks, I. E., Moore, T. S., Olsen, Y. S., Steckbauer, A., Ramajo, L., et al. (2013). Is ocean acidification an open-ocean syndrome? Understanding anthropogenic impacts on seawater pH. *Estuaries and Coasts*, *36*(2), 221–236. https://doi.org/10.1007/s12237-013-9594-3
Evans, C. D., Page, S. E., Jones, T., Moore, S., Gauci, V., Laiho, R., et al. (2014). Contrasting vulnerability of drained tropical and high-latitude peatlands to fluvial loss of stored carbon. *Global Biogeochemical Cycles*, *28*(11), 1215–1234. https://doi.org/10.1002/2013GB004782
Evans, C. D., Renou-Wilson, F., & Strack, M. (2016). The role of waterborne carbon in the greenhouse gas balance of drained and re-wetted peatlands. *Aquatic Sciences*, *78*(3), 573–590. https://doi.org/10.1007/s00027-015-0447-y
Fabricius, K. E., Langdon, C., Uthicke, S., Humphrey, C., Noonan, S., De'ath, G., et al. (2011). Losers and winners in coral reefs acclimatized to elevated carbon dioxide concentrations. *Nature Climate Change*, *1*(3), 165–169. https://doi.org/10.1038/nclimate1122
Fassbender, A., Orr, C. J., & Dickson, A. (2021). Technical note: Interpreting pH changes. *Biogeosciences*, *18*(4), 1407–1415. https://doi.org/10.5194/bg-18-1407-2021
Fichot, C. G., & Benner, R. (2014). The fate of terrigenous dissolved organic carbon in a river-influenced ocean margin. *Global Biogeochemical Cycles*, *28*(3), 300–318. https://doi.org/10.1002/2013GB004670

Follett, C. L., Repeta, D. J., Rothman, D. H., Xu, L., & Santinelli, C. (2014). Hidden cycle of dissolved organic carbon in the deep ocean. *Proceedings of the National Academy of Sciences of the United States of America*, *111*(47), 16706–16711. https://doi.org/10.1073/pnas.1407445111

Fransner, F., Fransson, A., Humborg, C., Gustafsson, E., Tedesco, L., Hordoir, R., & Nycander, J. (2019). Remineralization rate of terrestrial DOC as inferred from CO_2 supersaturated coastal waters. *Biogeosciences*, *16*(4), 863–879. https://doi.org/10.5194/bg-16-863-2019

Gandois, L., Hoyt, A. M., Mounier, S., Le Roux, G., Harvey, C. F., Claustres, A., et al. (2020). From canals to the coast: Dissolved organic matter and trace metal composition in rivers draining degraded tropical peatlands in Indonesia. *Biogeosciences*, *17*(7), 1897–1909. https://doi.org/10.5194/bg-17-1897-2020

Gandois, L., Teisserenc, R., Cobb, A. R., Chieng, H. I., Lim, L. B. L., Kamariah, A. S., et al. (2014). Origin, composition, and transformation of dissolved organic matter in tropical peatlands. *Geochimica et Cosmochimica Acta*, *137*, 35–47. https://doi.org/10.1016/j.gca.2014.03.012

Gordon, A. L., Huber, B. A., Metzger, E. J., Susanto, R. D., Hurlburt, H. E., & Adi, T. R. (2012). South China Sea throughflow impact on the Indonesian throughflow. *Geophysical Research Letters*, *39*(11). https://doi.org/10.1029/2012GL052021

Gran, G. (1952). Determination of the equivalence point in potentiometric titrations. Part II. *Analyst*, *77*, 661. https://doi.org/10.1039/AN9527700661

Guenet, B., Danger, M., Abbadie, L., & Lacroix, G. (2010). Priming effect: Bridging the gap between terrestrial and aquatic ecology. *Ecology*, *91*(10), 2850–2861. https://doi.org/10.1890/09-1968.1

Hadi, T., Muhammad, A., Giyanto, G., Prayudha, B., Johan, O., Budiyanto, A., et al. (2020). *The status of Indonesian coral reefs 2019*.

Hamzah, F., Agustiadi, T., Susanto, R. D., Wei, Z., Guo, L., Cao, Z., & Dai, M. (2020). Dynamics of the carbonate system in the western Indonesian seas during the southeast monsoon. *Journal of Geophysical Research: Oceans*, *125*(1), 1–18. https://doi.org/10.1029/2018JC014912

Helms, J. R., Stubbins, A., Ritchie, J. D., Minor, E. C., Kieber, D. J., & Mopper, K. (2008). Absorption spectral slopes and slope ratios as indicators of molecular weight, source, and photobleaching of chromophoric dissolved organic matter. *Limnology and Oceanography*, *53*(3), 955–969. https://doi.org/10.4319/lo.2008.53.3.0955

Hodgkins, S. B., Richardson, C. J., Dommain, R., Wang, H., Glaser, P. H., Verbeke, B., et al. (2018). Tropical peatland carbon storage linked to global latitudinal trends in peat recalcitrance. *Nature Communications*, *9*(1), 1–13. https://doi.org/10.1038/s41467-018-06050-2

Hoegh-Guldberg, O., Mumby, P. J., Hooten, A. J., Steneck, R. S., Greenfield, P., Gomez, E., et al. (2007). Coral reefs under rapid climate change and ocean acidification. *Science*, *318*(5857), 1737–1742. https://doi.org/10.1126/science.1152509

Huang, D., Tun, K. P. P., Chou, L. M., & Todd, P. a. (2009). An inventory of zooxanthellate scleractinian corals in Singapore, including 33 new records. *Raffles Bulletin of Zoology*, *22*(22), 69–80. Retrieved from http://rmbr.nus.edu.sg/rbz/biblio/s22/s22rbz069-080.pdf

Humborg, C., Geibel, M. C., Anderson, L. G., Björk, G., Mörth, C.-M., Sundbom, M., et al. (2017). Sea-air exchange patterns along the central and outer East Siberian Arctic Shelf as inferred from continuous CO_2, stable isotope, and bulk chemistry measurements. *Global Biogeochemical Cycles*, *31*(7), 1173–1191. https://doi.org/10.1002/2017GB005656

Humphreys, M. P., Greatrix, F. M., Tynan, E., Achterberg, E. P., Griffiths, A. M., Fry, C. H., et al. (2016). Stable carbon isotopes of dissolved inorganic carbon for a zonal transect across the subpolar North Atlantic Ocean in summer 2014. *Earth System Science Data*, *8*(1), 221–233. https://doi.org/10.5194/essd-8-221-2016

IPCC. (2014). *2013 supplement to the 2006 IPCC guidelines for national greenhouse gas inventories*. Intergovernmental Panel on Climate Change (IPCC).

Januchowski-Hartley, F. A., Bauman, A. G., Morgan, K. M., Seah, J. C. L., Huang, D., & Todd, P. A. (2020). Accreting coral reefs in a highly urbanized environment. *Coral Reefs*, *39*(3), 717–731. https://doi.org/10.1007/s00338-020-01953-3

Kaiser, K., Benner, R., & Amon, R. M. W. (2017). The fate of terrigenous dissolved organic carbon on the Eurasian shelves and export to the North Atlantic. *Journal of Geophysical Research: Oceans*, *122*(1), 4–22. https://doi.org/10.1002/2016JC012380

Kitidis, V., Shutler, J. D., Ashton, I., Warren, M., Brown, I., Findlay, H., et al. (2019). Winter weather controls net influx of atmospheric CO_2 on the north-west European shelf. *Scientific Reports*, *9*(1), 1–11. https://doi.org/10.1038/s41598-019-56363-5

Kleypas, J. A., McManu, J. W., & Mene, L. A. B. (1999). Environmental limits to coral reef development: Where do we draw the line? *American Zoologist*, *39*(1), 146–159. https://doi.org/10.1093/icb/39.1.146

Langdon, C. (2005). Effect of elevated pCO_2 on photosynthesis and calcification of corals and interactions with seasonal change in temperature/irradiance and nutrient enrichment. *Journal of Geophysical Research*, *110*(C9), C09S07. https://doi.org/10.1029/2004JC002576

Letscher, R. T., Hansell, D. A., & Kadko, D. (2011). Rapid removal of terrigenous dissolved organic carbon over the Eurasian shelves of the Arctic Ocean. *Marine Chemistry*, *123*(1–4), 78–87. https://doi.org/10.1016/j.marchem.2010.10.002

Lønborg, C., Calleja, M. L., Fabricius, K. E., Smith, J. N., & Achterberg, E. P. (2019). The Great Barrier Reef: A source of CO_2 to the atmosphere. *Marine Chemistry*, *210*, 24–33. https://doi.org/10.1016/j.marchem.2019.02.003

Manzello, D. P., Kleypas, J. A., Budd, D. A., Eakin, C. M., Glynn, P. W., & Langdon, C. (2008). Poorly cemented coral reefs of the eastern tropical Pacific: Possible insights into reef development in a high-CO_2 world. *Proceedings of the National Academy of Sciences of the United States of America*, *105*(30), 10450–10455. https://doi.org/10.1073/pnas.0712167105

Martin, P., Cherukuru, N., Tan, A. S. Y., Sanwlani, N., Mujahid, A., & Müller, M. (2018). Distribution and cycling of terrigenous dissolved organic carbon in peatland-draining rivers and coastal waters of Sarawak, Borneo. *Biogeosciences*, *15*(22), 6847–6865. https://doi.org/10.5194/bg-15-6847-2018

Martin, P., Sanwlani, N., Wan, T., Lee, Q., Meng, J., & Wong, C. (in press). Dissolved organic matter from tropical peatlands impacts shelf sea light availability in the Singapore Strait, Southeast Asia. *Marine Ecology Progress Series*. https://doi.org/10.3354/meps13776

Mayer, B., & Pohlmann, T. (2014). Simulation of organic pollutants: First step towards an adaptation to the Malacca strait. *Asian Journal of Water, Environment and Pollution*, *11*(1), 75–86.

Mayer, B., Rixen, T., & Pohlmann, T. (2018). The spatial and temporal variability of air-sea CO_2 fluxes and the effect of net coral reef calcification in the Indonesian Seas: A numerical sensitivity study. *Frontiers in Marine Science*, *5*, 1–19. https://doi.org/10.3389/fmars.2018.00116

Mayer, B., Stacke, T., Stottmeister, I., & Pohlmann, T. (2015). Sunda Shelf Seas: Flushing rates and residence times. *Ocean Science Discussions*, *12*(3), 863–895. https://doi.org/10.5194/osd-12-863-2015

Medeiros, P. M., Seidel, M., Niggemann, J., Spencer, R. G. M., Hernes, P. J., Yager, P. L., et al. (2016). A novel molecular approach for tracing terrigenous dissolved organic matter into the deep ocean. *Global Biogeochemical Cycles*, *30*(5), 689–699. https://doi.org/10.1002/2015GB005320

Medeiros, P. M., Seidel, M., Ward, N. D., Carpenter, E. J., Gomes, H. R., Niggemann, J., et al. (2015). Fate of the Amazon River dissolved organic matter in the tropical Atlantic Ocean. *Global Biogeochemical Cycles*, *29*(5), 677–690. https://doi.org/10.1002/2015GB005115

Mehrbach, C., Culberson, C. H., Hawley, J. E., & Pytkowicx, R. M. (1973). Measurement of the apparent dissociation constants of carbonic acid in seawater at atmospheric pressure. *Limnology and Oceanography*, *18*(6), 897–907. https://doi.org/10.4319/lo.1973.18.6.0897

Melzner, F., Thomsen, J., Koeve, W., Oschlies, A., Gutowska, M. A., Bange, H. W., et al. (2013). Future ocean acidification will be amplified by hypoxia in coastal habitats. *Marine Biology*, *160*(8), 1875–1888. https://doi.org/10.1007/s00227-012-1954-1

Meybeck, M. (1982). Carbon, nitrogen, and phosphorus transport by world rivers. *American Journal of Science*, *282*(4), 401–450. https://doi.org/10.2475/ajs.282.4.401

Meyers-Schulte, K. J., & Hedges, J. I. (1986). Molecular evidence for a terrestrial component of organic matter dissolved in ocean water. *Nature*, *321*(6065), 61–63. https://doi.org/10.1038/321061a0

Miettinen, J., Shi, C., & Liew, S. C. (2016). Land cover distribution in the peatlands of Peninsular Malaysia, Sumatra and Borneo in 2015 with changes since 1990. *Global Ecology and Conservation*, *6*, 67–78. https://doi.org/10.1016/j.gecco.2016.02.004

Mollica, N. R., Guo, W., Cohen, A. L., Huang, K. F., Foster, G. L., Donald, H. K., & Solow, A. R. (2018). Ocean acidification affects coral growth by reducing skeletal density. *Proceedings of the National Academy of Sciences of the United States of America*, *115*(8), 1754–1759. https://doi.org/10.1073/pnas.1712806115

Moore, S., Evans, C. D., Page, S. E., Garnett, M. H., Jones, T. G., Freeman, C., et al. (2013). Deep instability of deforested tropical peatlands revealed by fluvial organic carbon fluxes. *Nature*, *493*(7434), 660–663. https://doi.org/10.1038/nature11818

Moore, S., Gauci, V., Evans, C. D., & Page, S. E. (2011). Fluvial organic carbon losses from a Bornean blackwater river. *Biogeosciences*, *8*(4), 901–909. https://doi.org/10.5194/bg-8-901-2011

Moran, M. A., Sheldon, W. M., & Zepp, R. G. (2000). Carbon loss and optical property changes during long-term photochemical and biological degradation of estuarine dissolved organic matter. *Limnology and Oceanography*, *45*(6), 1254–1264. https://doi.org/10.4319/lo.2000.45.6.1254

Moran, M. A., & Zepp, R. G. (1997). Role of photoreactions in the formation of biologically labile compounds from dissolved organic matter. *Limnology and Oceanography*, *42*(6), 1307–1316. https://doi.org/10.4319/lo.1997.42.6.1307

Morgan, K. M., Moynihan, M. A., Sanwlani, N., & Switzer, A. D. (2020). Light limitation and depth-variable sedimentation drives vertical reef compression on turbid coral reefs. *Frontiers in Marine Science*, *7*, 1–13. https://doi.org/10.3389/fmars.2020.571256

Müller, D., Warneke, T., Rixen, T., Müller, M., Jamahari, D., Denis, N., et al. (2015). Lateral carbon fluxes and CO_2 outgassing from a tropical peat-draining river. *Biogeosciences*, *12*(20), 5967–5979. https://doi.org/10.5194/bg-12-5967-2015

Müller-Dum, D., Warneke, T., Rixen, T., Müller, M., Baum, A., Christodoulou, A., et al. (2019). Impact of peatlands on carbon dioxide (CO_2) emissions from the Rajang River and Estuary, Malaysia. *Biogeosciences*, *16*(1), 17–32. https://doi.org/10.5194/bg-16-17-2019

Nichols, R. S., & Martin, P. (2021). Low biodegradability of dissolved organic matter from Southeast Asian peat-draining rivers. *Journal of Geophysical Research: Biogeosciences*. https://doi.org/10.1029/2020jg006182

Opsahl, S., & Benner, R. (1997). Distribution and cycling of terrigenous dissolved organic matter in the ocean. *Nature*, *386*(6624), 480–482. https://doi.org/10.1038/386480a0

Opsahl, S., & Zepp, R. G. (2001). Photochemically-induced alteration of stable carbon isotope ratios ($\delta_{13}C$) in terrigeneous dissolved organic carbon. *Geophysical Research Letters*, *28*(12), 2417–2420. https://doi.org/10.1029/2000GL012686

Orr, J. C., Epitalon, J. M., Dickson, A. G., & Gattuso, J. P. (2018). Routine uncertainty propagation for the marine carbon dioxide system. *Marine Chemistry*, *207*, 84–107. https://doi.org/10.1016/j.marchem.2018.10.006

Osburn, C. L., Morris, D. P., Thorn, K. A., & Moeller, R. E. (2001). Chemical and optical changes in freshwater dissolved organic matter exposed to solar radiation. *Biogeochemistry*, *54*(3), 251–278. https://doi.org/10.1023/A:1010657428418

Pacella, S. R., Brown, C. A., Waldbusser, G. G., Labiosa, R. G., & Hales, B. (2018). Seagrass habitat metabolism increases short-term extremes and long-term offset of CO_2 under future ocean acidification. *Proceedings of the National Academy of Sciences of the United States of America*, *115*(15), 3870–3875. https://doi.org/10.1073/pnas.1703445115

Page, S. E., Rieley, J. O., & Banks, C. J. (2011). Global and regional importance of the tropical peatland carbon pool. *Global Change Biology*, *17*(2), 798–818. https://doi.org/10.1111/j.1365-2486.2010.02279.x

Painter, S. C., Lapworth, D. J., Woodward, E. M. S., Kroeger, S., Evans, C. D., Mayor, D. J., & Sanders, R. J. (2018). Terrestrial dissolved organic matter distribution in the North Sea. *Science of the Total Environment*, *630*, 630–647. https://doi.org/10.1016/j.scitotenv.2018.02.237

Pisapia, C., Hochberg, E. J., & Carpenter, R. (2019). Multi-decadal change in reef-scale production and calcification associated with recent disturbances on a Lizard Island reef flat. *Frontiers in Marine Science*, *6*, 1–10. https://doi.org/10.3389/fmars.2019.00575

Rixen, T., Baum, A., Pohlmann, T., Balzer, W., Samiaji, J., & Jose, C. (2008). The Siak, a tropical black water river in central Sumatra on the verge of anoxia. *Biogeochemistry*, *90*(2), 129–140. https://doi.org/10.1007/s10533-008-9239-y

Rixen, T., Baum, A., Wit, F., & Samiaji, J. (2016). Carbon leaching from tropical peat soils and consequences for carbon balances. *Frontiers in Earth Science*, *4*. https://doi.org/10.3389/feart.2016.00074

Roobaert, A., Laruelle, G. G., Landschützer, P., Gruber, N., Chou, L., & Regnier, P. (2019). The spatiotemporal dynamics of the sources and sinks of CO_2 in the Global Coastal Ocean. *Global Biogeochemical Cycles*, *2*, 1–22. https://doi.org/10.1029/2019GB006239

Samanta, S., Dalai, T. K., Pattanaik, J. K., Rai, S. K., & Mazumdar, A. (2015). Dissolved inorganic carbon (DIC) and its $\delta^{13}C$ in the Ganga (Hooghly) River estuary, India: Evidence of DIC generation via organic carbon degradation and carbonate dissolution. *Geochimica et Cosmochimica Acta*, *165*, 226–248. https://doi.org/10.1016/j.gca.2015.05.040

Semiletov, I., Pipko, I., Gustafsson, Ö., Anderson, L. G., Sergienko, V., Pugach, S., et al. (2016). Acidification of East Siberian Arctic Shelf waters through addition of freshwater and terrestrial carbon. *Nature Geoscience*, *9*(5), 361–365. https://doi.org/10.1038/NEGO269510.1038/ngeo2695

Shirokova, L. S., Chupakov, A. V., Zabelina, S. A., Neverova, N. V., Payandi-Rolland, D., Causserand, C., et al. (2019). Humic surface waters of frozen peat bogs (permafrost zone) are highly resistant to bio- and photodegradation. *Biogeosciences*, *16*(12), 2511–2526. https://doi.org/10.5194/bg-16-2511-2019

Siegel, H., Gerth, M., Stottmeister, I., Baum, A., & Samiaji, J. (2019). Remote sensing of coastal discharge of SE Sumatra (Indonesia). In Remote sensing of the Asian Seas (pp. 359–376). Springer International Publishing. https://doi.org/10.1007/978-3-319-94067-0_20

Spencer, R. G. M., Stubbins, A., Hernes, P. J., Baker, A., Mopper, K., Aufdenkampe, A. K., et al. (2009). Photochemical degradation of dissolved organic matter and dissolved lignin phenols from the Congo River. *Journal of Geophysical Research*, *114*, G03010. https://doi.org/10.1029/2009JG000968

Stoltenberg, L., Schulz, K. G., Lantz, C. A., Cyronak, T., & Eyre, B. D. (2021). Late afternoon seasonal transition to dissolution in a coral reef: An early warning of a net dissolving ecosystem? *Geophysical Research Letters*, *48*. https://doi.org/10.1029/2020gl090811

Stubbins, A., Mann, P. J., Powers, L., Bittar, T. B., Dittmar, T., McIntyre, C. P., et al. (2017). Low photolability of yedoma permafrost dissolved organic carbon. *Journal of Geophysical Research: Biogeosciences*, *122*(1), 200–211. https://doi.org/10.1002/2016JG003688

Stubbins, A., Spencer, R. G. M., Chen, H., Hatcher, P. G., Mopper, K., Hernes, P. J., et al. (2010). Illuminated darkness: Molecular signatures of Congo River dissolved organic matter and its photochemical alteration as revealed by ultrahigh precision mass spectrometry. *Limnology and Oceanography*, *55*(4), 1467–1477. https://doi.org/10.4319/lo.2010.55.4.1467

Tranvik, L. J., Downing, J. A., Cotner, J. B., Loiselle, S. A., Striegl, R. G., Ballatore, T. J., et al. (2009). Lakes and reservoirs as regulators of carbon cycling and climate. *Limnology and Oceanography*, *54*(6 part 2), 2298–2314. https://doi.org/10.4319/lo.2009.54.6_part_2.2298

UNEP-WCMC. (2010). *Global distribution of warm-water coral reefs, compiled from multiple sources including the Millennium Coral Reef Mapping Project, Version 1.3*.

Uppström, L. R. (1974). The boron/chlorinity ratio of deep-sea water from the Pacific Ocean. *Deep-Sea Research and Oceanographic Abstracts*, *21*(2), 161–162. https://doi.org/10.1016/0011-7471(74)90074-6

van Heuven, S., Pierrot, D., Rae, J. W. B., Lewis, E., & Wallace, D. W. R. (2011). *MATLAB program developed for CO_2 system calculations* (ORNL/CDIAC-105b). Carbon Dioxide Information Analysis Center, Oak Ridge National Laboratory, U.S. Department of Energy. https://doi.org/10.3334/CDIAC/otg.CO2SYS_MATLAB_v1.1

van Nugteren, P., Moodley, L., Brummer, G. J., Heip, C. H. R., Herman, P. M. J., & Middelburg, J. J. (2009). Seafloor ecosystem functioning: The importance of organic matter priming. *Marine Biology*, *156*(11), 2277–2287. https://doi.org/10.1007/s00227-009-1255-5

Wanninkhof, R. (2014). Relationship between wind speed and gas exchange over the ocean revisited. *Limnology and Oceanography: Methods*, *12*(6), 351–362. https://doi.org/10.4319/lom.2014.12.351

Ward, C. P., Nalven, S. G., Crump, B. C., Kling, G. W., & Cory, R. M. (2017). Photochemical alteration of organic carbon draining permafrost soils shifts microbial metabolic pathways and stimulates respiration. *Nature Communications*, *8*(1), 1–7. https://doi.org/10.1038/s41467-017-00759-2

Ward, N. D., Keil, R. G., Medeiros, P. M., Brito, D. C., Cunha, A. C., Dittmar, T., et al. (2013). Degradation of terrestrially derived macromolecules in the Amazon River. *Nature Geoscience*, *6*(7), 530–533. https://doi.org/10.1038/ngeo1817

Weishaar, J. L., Aiken, G. R., Bergamaschi, B. A., Fram, M. S., Fujii, R., & Mopper, K. (2003). Evaluation of specific ultraviolet absorbance as an indicator of the chemical composition and reactivity of dissolved organic carbon. *Environmental Science & Technology*, *37*(20), 4702–4708. https://doi.org/10.1021/es030360x

Weiss, R. F. (1974). Carbon dioxide in water and seawater: The solubility of a non-ideal gas. *Marine Chemistry*, *2*(3), 203–215. https://doi.org/10.1016/0304-4203(74)90015-2

Welschmeyer, N. A. (1994). Fluorometric analysis of chlorophyll a in the presence of chlorophyll b and pheopigments. *Limnology and Oceanography*, *39*(8), 1985–1992. https://doi.org/10.4319/lo.1994.39.8.1985

Wickland, K. P., Neff, J. C., & Aiken, G. R. (2007). Dissolved organic carbon in Alaskan boreal forest: Sources, chemical characteristics, and biodegradability. *Ecosystems*, *10*(8), 1323–1340. https://doi.org/10.1007/s10021-007-9101-4

Wilson, S., Blain, D., Couwenberg, J., Evans, C. D., Murdiyarso, D., Page, S. E., et al. (2016). Greenhouse gas emission factors associated with rewetting of organic soils. *Mires and Peat*, *17*(4), 1–28. https://doi.org/10.19189/MaP.2016.OMB.222

Wit, F., Müller, D., Baum, A., Warneke, T., Pranowo, W. S., Müller, M., & Rixen, T. (2015). The impact of disturbed peatlands on river outgassing in Southeast Asia. *Nature Communications*, *6*, 10155. https://doi.org/10.1038/ncomms10155

Wit, F., Rixen, T., Baum, A., Pranowo, W. S., & Hutahaean, A. A. (2018). The Invisible Carbon Footprint as a hidden impact of peatland degradation inducing marine carbonate dissolution in Sumatra, Indonesia. *Scientific Reports*, *8*(1), 17403. https://doi.org/10.1038/s41598-018-35769-7

Yupi, H. M., Inoue, T., Bathgate, J., & Putra, R. (2016). Concentrations, loads and yields of organic carbon from two tropical peat swamp forest streams in Riau province, Sumatra, Indonesia. *Mires and Peat*, *18*, 1–15. https://doi.org/10.19189/MaP.2015.OMB.181

Zeebe, R. E., & Wolf-Gladrow, D. A. (2001). *CO_2 in seawater: Equilibrium, kinetics, isotopes*. Elsevier Oceanography Series.

Zhou, Y., Martin, P., & Müller, M. (2019). Composition and cycling of dissolved organic matter from tropical peatlands of coastal Sarawak, Borneo, revealed by fluorescence spectroscopy and parallel factor analysis. *Biogeosciences*, *16*(13), 2733–2749. https://doi.org/10.5194/bg-16-2733-2019

Zhu, Z.-Y., Oakes, J., Eyre, B., Hao, Y., Sia, E. S. A., Jiang, S., et al. (2020). The nonconservative distribution pattern of organic matter in the Rajang, a tropical river with peatland in its estuary. *Biogeosciences*, *17*(9), 2473–2485. https://doi.org/10.5194/bg-17-2473-2020

Zigah, P. K., McNichol, A. P., Xu, L., Johnson, C., Santinelli, C., Karl, D. M., & Repeta, D. J. (2017). Allochthonous sources and dynamic cycling of ocean dissolved organic carbon revealed by carbon isotopes. *Geophysical Research Letters*, *44*(5), 2407–2415. https://doi.org/10.1002/2016GL071348

References From the Supporting Information

IAEA. (1993). *Reference and intercomparison materials for stable isotopes of light elements*. Proceedings of a Consultants meeting held in Vienna. https://doi.org/10.1016/0020-708X(73)90108-7

Rau, G. H., Riebesell, U., & Wolf-Gladrow, D. (1996). A model of photosynthetic 13C fractionation by marine phytoplankton based on diffusive molecular CO_2 uptake. *Marine Ecology Progress Series*, *133*(1–3), 275–285. https://doi.org/10.3354/meps133275

Su, J., Cai, W. J., Hussain, N., Brodeur, J., Chen, B., & Huang, K. (2019). Simultaneous determination of dissolved inorganic carbon (DIC) concentration and stable isotope (δ13C-DIC) by Cavity Ring-Down Spectroscopy: Application to study carbonate dynamics in the Chesapeake Bay. *Marine Chemistry*, *215*, 103689. https://doi.org/10.1016/j.marchem.2019.103689